The Transcription Factor Pdr802 Regulates Titan Cell Formation and Pathogenicity of *Cryptococcus neoformans*

Julia C. V. Reuwsaat,[a,b] Daniel P. Agustinho,[b] Heryk Motta,[a] Andrew L. Chang,[b] Holly Brown,[b] Michael R. Brent,[c,d,e] Livia Kmetzsch,[a,f] Tamara L. Doering[b]

aMolecular Biology of Pathogens Laboratory, Biotechnology Center, Universidade Federal do Rio Grande do Sul, Porto Alegre, Brazil
bDepartment of Molecular Microbiology, Washington University School of Medicine, St. Louis, Missouri, USA
cCenter for Genome Sciences and Systems Biology, Washington University School of Medicine, St. Louis, Missouri, USA
dDepartment of Computer Science and Engineering, Washington University, St. Louis, Missouri, USA
eDepartment of Genetics, Washington University, St. Louis, Missouri, USA
fDepartment of Molecular Biology and Biotechnology, Universidade Federal do Rio Grande do Sul, Porto Alegre, Brazil

ABSTRACT *Cryptococcus neoformans* is a ubiquitous, opportunistic fungal pathogen that kills almost 200,000 people worldwide each year. It is acquired when mammalian hosts inhale the infectious propagules; these are deposited in the lung and, in the context of immunocompromise, may disseminate to the brain and cause lethal meningoencephalitis. Once inside the host, *C. neoformans* undergoes a variety of adaptive processes, including secretion of virulence factors, expansion of a polysaccharide capsule that impedes phagocytosis, and the production of giant (Titan) cells. The transcription factor Pdr802 is one regulator of these responses to the host environment. Expression of the corresponding gene is highly induced under host-like conditions *in vitro* and is critical for *C. neoformans* dissemination and virulence in a mouse model of infection. Direct targets of Pdr802 include the quorum sensing proteins Pqp1, Opt1, and Liv3; the transcription factors Stb4, Zfc3, and Bzp4, which regulate cryptococcal brain infectivity and capsule thickness; the calcineurin targets Had1 and Crz1, important for cell wall remodeling and *C. neoformans* virulence; and additional genes related to resistance to host temperature and oxidative stress, and to urease activity. Notably, cryptococci engineered to lack Pdr802 showed a dramatic increase in Titan cells, which are not phagocytosed and have diminished ability to directly cross biological barriers. This explains the limited dissemination of *pdr802* mutant cells to the central nervous system and the consequently reduced virulence of this strain. The role of Pdr802 as a negative regulator of Titan cell formation is thus critical for cryptococcal pathogenicity.

IMPORTANCE The pathogenic yeast *Cryptococcus neoformans* presents a worldwide threat to human health, especially in the context of immunocompromise, and current antifungal therapy is hindered by cost, limited availability, and inadequate efficacy. After the infectious particle is inhaled, *C. neoformans* initiates a complex transcriptional program that integrates cellular responses and enables adaptation to the host lung environment. Here, we describe the role of the transcription factor Pdr802 in the response to host conditions and its impact on *C. neoformans* virulence. We identified direct targets of Pdr802 and also discovered that it regulates cellular features that influence movement of this pathogen from the lung to the brain, where it causes fatal disease. These findings significantly advance our understanding of a serious disease.

KEYWORDS *Cryptococcus neoformans*, Pdr802, Titan cells, capsule, fungal pathogens, pathogenesis, pathogenic yeast, quorum sensing, transcription factors

Address correspondence to Livia Kmetzsch, livia.kmetzsch@ufrgs.br, or Tamara L. Doering, doering@wustl.edu.

Cryptococcosis is a fungal infection caused by *Cryptococcus neoformans* and *Cryptococcus gattii*. *C. neoformans* is a ubiquitous opportunistic pathogen that infects mainly immunocompromised patients, while *C. gattii* is capable of infecting immunocompetent individuals (1). Cryptococcosis causes 180,000 deaths worldwide each year, including roughly 15% of all AIDS-related deaths (2), and is initiated by the inhalation of spores or desiccated yeast cells. In immunocompetent individuals, this typically causes an asymptomatic pulmonary infection that is controlled by the host immune response, although a population of *C. neoformans* may remain latent for extended periods of time (3–5).

Under conditions of immunocompromise, cryptococci disseminate from the lung to the brain. Mechanisms that have been suggested to mediate fungal crossing of the blood-brain barrier (BBB) include transcellular migration, in which the yeast cells enter and exit vascular endothelial cells (6–9); paracellular movement, in which they cross the BBB at junctions between endothelial cells (10–12); and "Trojan horse" crossing, whereby macrophages harboring *C. neoformans* enter the brain (13). Cryptococcal meningoencephalitis is difficult to treat and frequently lethal, for reasons that include the availability and cost of therapy (14, 15).

The ability of *C. neoformans* to survive and proliferate in the lung, and subsequently disseminate to the brain, depends on viability at mammalian body temperature and the expression of multiple virulence traits; these include secreted factors (16, 17), a polysaccharide capsule that surrounds the cell wall (18), and the production of giant (Titan) cells (19, 20). One secreted molecule, the pigment melanin, associates with the cell wall, where its antioxidant properties protect fungal cells from reactive oxygen species produced as a host immune defense (21–25). Urease, a secreted metalloenzyme that converts urea to ammonia and CO_2, may affect the course of infection by modulating environmental pH and damaging host tissue structure (11, 12, 26).

The capsule, composed primarily of large polysaccharides (27–29), is a key cryptococcal virulence factor that impairs phagocytosis by immune cells (30–35). This dynamic entity changes its size and structure during interactions with the host or external environment (36–39), contributing to fungal adaptation (40, 41). Capsule polysaccharides that are shed from the cell enable diagnosis of cryptococcal infection and also impede host responses (35, 42).

Titan cells are a cryptococcal morphotype that has been variously characterized as having a cell body diameter (excluding the capsule) greater than 10 or 15 μm or total cell diameter (including the capsule) that exceeds 30 μm (20, 43, 44). These cells are polyploid and produce normal-size cells during infection (19, 45, 46). Titan cell formation is triggered by exposure to the host environment, including nutrient starvation, reduced pH, and hypoxia (47–49), although the extent of induction depends on the host immune response and the duration of infection (45, 50). Titan cell production appears to benefit the development of pulmonary *C. neoformans* infection, since these large cells are less susceptible to internalization by host phagocytes and more resistant to oxidative stress than normal-size cells (19, 46). Some of these effects may be explained by the highly cross-linked capsule and thickened cell wall of Titan cells (51). In contrast to their success in the lungs, Titan cells show impaired dissemination to the brain (19, 46).

C. neoformans experiences a dramatic change in conditions upon entering a host, including altered nutrient levels and pH. To adapt to the new environment, cryptococci activate a network of transcription factors (TFs) (39, 52). For example, imbalances in ion homeostasis trigger transcriptional changes mediated by the TFs Zap1 (53), Cuf1 (54), Pho4 (55), Cir1 (56), and Crz1 (57). Alkaline pH stimulates expression of the TF Rim101, which enables growth under basic conditions and other stresses, such as high salt and iron limitation; it also promotes the association of capsule polysaccharide with the cell and the formation of Titan cells (47, 58).

Overlapping TF circuits regulate cryptococcal virulence determinants, including polysaccharide capsule production and melanin synthesis. For example, Usv101, an

important regulator of capsule thickness and polysaccharide shedding, also regulates three other TFs (Gat201, Crz1, and Rim101) and multiple polysaccharide-related enzymes (59). Gat201 further regulates additional virulence-related transcription factors and the anti-phagocytic protein Blp1 (60), while Crz1 plays a central role in the maintenance of plasma membrane and cell wall stability (57, 61, 62). Crz1 expression is also modulated by the calcineurin signaling pathway, which is required for normal yeast growth at 37°C, virulence, and sexual reproduction (63). A group of TFs, including Usv101, Bzp4, Hob1, and Mbs1 (59, 64), act together to regulate melanin production; deletion of Bzp4 also alters capsule production (52).

In this study, we investigated the TF Pdr802. The corresponding gene has a high rate of nonsynonymous mutations, which suggests that it is evolving rapidly (65). Pdr802 has previously been implicated in *C. neoformans* virulence (39, 52, 66), but its specific role and targets are not known. We discovered that Pdr802 is induced under host-like conditions, is a negative regulator of Titan cell formation, and influences capsule thickness and phagocytosis by macrophages. It also regulates genes whose products act in cell wall remodeling, virulence factor production, resistance to host temperature and oxidative stress, and quorum sensing. These functions make Pdr802 critical for cryptococcal survival in the lung and dissemination to the brain.

RESULTS

Role of Pdr802 in *C. neoformans* virulence. The importance of Pdr802 in *C. neoformans* virulence has been demonstrated in multiple experimental models. Liu and collaborators first reported in 2008 that partial deletion of *PDR802* reduced *C. neoformans* infectivity in a competition assay of pooled *C. neoformans* strains (66). In 2015, Maier et al. showed that a *pdr802* deletion mutant had reduced virulence when tested individually in a short-term mouse model of infection (39). Later that year, Jung and colleagues reported that Pdr802 was required for full virulence in both wax moth larva and short-term mouse infection using pooled strains (52). Most recently, Lee and collaborators showed that Pdr802 was required for brain infection (67).

To further investigate the role of Pdr802 in pathogenesis, we complemented a complete deletion strain in the KN99α background that we had previously generated (*pdr802*) (39) with the intact gene at its native locus (*PDR802*). To examine targets of Pdr802, we also constructed a strain that expresses the protein fused to mCherry at its N terminus (see Fig. S1A in the supplemental material). All of these strains lacked or expressed RNA encoding *PDR802* or its modified forms as expected (Fig. S1B), and *PDR802* was expressed at wild-type levels in the complemented and modified strains (Fig. S1C).

We next assessed the long-term survival of C57BL/6 mice infected with the parental wild-type (WT) strain (KN99α), the deletion mutant (*pdr802*), or the complemented mutant (*PDR802*). In this model, mice infected with the parent or complemented strains survived for roughly 3 weeks, while those infected with the deletion mutant showed a striking increase in survival: all animals survived for at least 65 days, and over half survived to the end of the study (100 days) (Fig. 1A). The lung burden measured at the time of death for *pdr802*-infected mice in this study was approximately 100-fold lower than that of wild-type infections (Fig. S2A), demonstrating the importance of this TF in *C. neoformans* virulence. Mean brain burden at the time of death was more similar between mutant and wild-type infections (Fig. S2A), although we did note some heterogeneity in this measure for *pdr802*-infected mice; animals sacrificed at around 2 months of infection (red symbols) showed brain burdens similar to WT levels, while brain burdens in mice sacrificed at day 100 (blue symbols) ranged between zero fungal cells and the WT level.

We next examined the time course of fungal proliferation in the lungs. As expected, the burdens of WT and the complemented mutant strains increased steadily over an 18-day interval (Fig. 1B), eventually reaching roughly 10^5 times the original inoculum. Towards the end of this period, these cells were also detected in the blood and brain
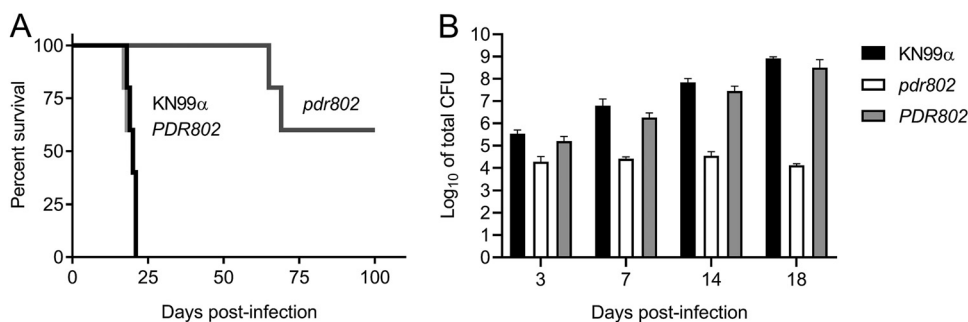
FIG 1 The transcription factor Pdr802 influences *C. neoformans* virulence. (A) Survival of C57BL/6 mice over time after intranasal inoculation with 5×10^4 cryptococci, with sacrifice triggered by weight below 80% of peak. (B) Means and standard deviations (SD) of total colony-forming units (CFU) in lung tissue at various times post-infection. Numbers of CFU inoculated for each strain were 41,400 (KN99α), 42,800 (*pdr802* strain) and 26,600 (*PDR802* strain). $P < 0.05$ for the *pdr802* strain compared to the other strains at all time points.

(Fig. S2B). In contrast, the lung burden of *pdr802* remained close to the inoculum throughout this period, with no mutant cells detected in the blood or brain. At a late time point of *pdr802* infection (75 days), we again noted some heterogeneity of fungal burden: one mouse had high lung burden with no dissemination, another had high lung burden with moderate brain burden, and the third had extremely low lung burden with no dissemination (Fig. S2C). No CFU were detected in the blood of *pdr802*-infected mice at any point during infection. These results suggest that even though the *pdr802* mutant is generally hypovirulent and remains at low levels in the lung, it can occasionally reach the brain and, given enough time, accumulate there (see Discussion).

Given the dramatic effects of Pdr802 on fungal virulence, we wondered about the specific biological processes in which this transcription factor is involved. We first examined the behavior of the *pdr802* strain *in vitro*, including stress conditions that might be encountered in the host. We saw no differences in growth of the mutant compared to WT cells under conditions that challenge cell or cell wall integrity, including the presence of sorbitol, high salt, cell wall dyes, caffeine, sodium dodecyl sulfate (SDS), or ethanol (Fig. S3A to C). The mutant also showed no altered susceptibility to elements of the host response, such as nitrosative or oxidative stresses, or in melanin production. All of these results held when cells were grown on rich medium, whether plates were incubated at 30°C, 37°C, or 37°C in the presence of 5% CO_2, which was recently described as an independent stress for *C. neoformans* (68) (Fig. S3A to C). Finally, the mutant showed no difference from wild-type cells in secretion of urease (Fig. S3D).

Pdr802 is regulated by "host-like" conditions. We next tested the growth of the *pdr802* mutant under conditions more like those encountered inside the mammalian host, using tissue culture medium (Dulbecco's modified Eagle medium [DMEM]) at 37°C in the presence of 5% CO_2. We found that although the *pdr802* mutant grew like WT in rich medium (yeast extract-peptone-dextrose [YPD]), it grew poorly in DMEM (Fig. S4A and B). To test whether the mutant cells were dead or just static after growth in DMEM, we plated aliquots on solid medium to measure CFU over time (Fig. 2A). The *pdr802* culture showed a dramatic decrease in viability compared to WT and the complemented strain, which was greatest in the first 24 h. This is the same time frame in which expression of the *PDR802* gene shows a striking increase, as measured by transcriptome sequencing (RNA-Seq) (Fig. 2B).

Another important feature that is induced by growth in DMEM at 37°C and 5% CO_2 is the polysaccharide capsule, which we previously reported to be regulated by Pdr802, based on negative staining with India ink (39). Fluorescence microscopy confirmed increased capsule thickness of the mutant, which reverted to WT in the
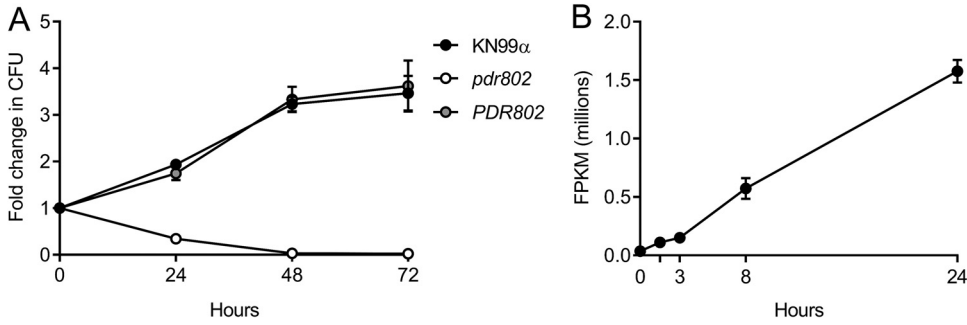
FIG 2 *PDR802* expression is required for cell viability and induced during growth under host-like conditions. (A) Cells grown in DMEM at 37°C and 5% CO_2 were sampled at the times indicated and plated on YPD to assess viability (measured as number of CFU and plotted as fold change from time zero). (B) *PDR802* expression in KN99α cells grown in DMEM at 37°C and 5% CO_2 was assessed by RNA-Seq as in reference 117. FPKM, fragments per kilobase per million. Mean and standard deviation (SD) are shown on both plots.

complemented strain (Fig. 3A). To quantify this change, we took advantage of a semi-automated assay that we have developed (Fig. S5), which measures capsules on a population scale (Fig. 3B) and is therefore very sensitive. This analysis showed that the capsule thickness of *pdr802* cells resembles that of the well-studied hypercapsular mutant *pkr1* (39, 69, 70) and is completely restored to WT by complementation at the native locus (Fig. 3C). Previous studies suggest that capsule thickness upon induction reflects the size of the dominant capsule polymer (glucuronoxylomannan [GXM]) (71, 72), which can be analyzed by agarose gel migration and blotting with anticapsule antibodies (71). Consistent with the difference we observed in capsule thickness by imaging, this method showed decreased mobility of GXM from *pdr802* as capsule induction progressed (Fig. S4C).
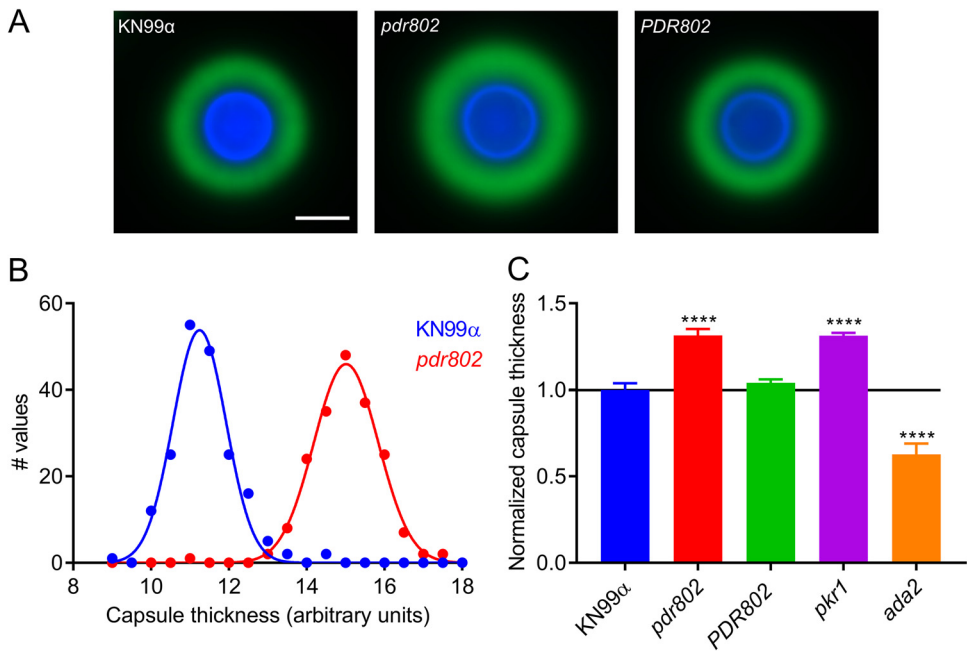
FIG 3 The *pdr802* mutant is hypercapsular. (A) Representative immunofluorescence micrographs of the indicated strains after growth in DMEM (37°C, 5% CO_2) for 24 h. The capsule was stained with anti-GXM monoclonal antibody 302 conjugated with Alexa Fluor 488 (green) and the cell wall with calcofluor white (blue). All images are to the same scale; bar, 5 μm. (B) Capsule thickness distribution for the indicated strains. (C) Mean and SD of capsule size, quantified as detailed in Materials and Methods and Fig. S5, with the *pkr1* (39) and *ada2* (105) strains shown as hypercapsular and hypocapsular controls, respectively. ****, $P < 0.0001$, compared to KN99α by one-way ANOVA with a *post hoc* Dunnett test.
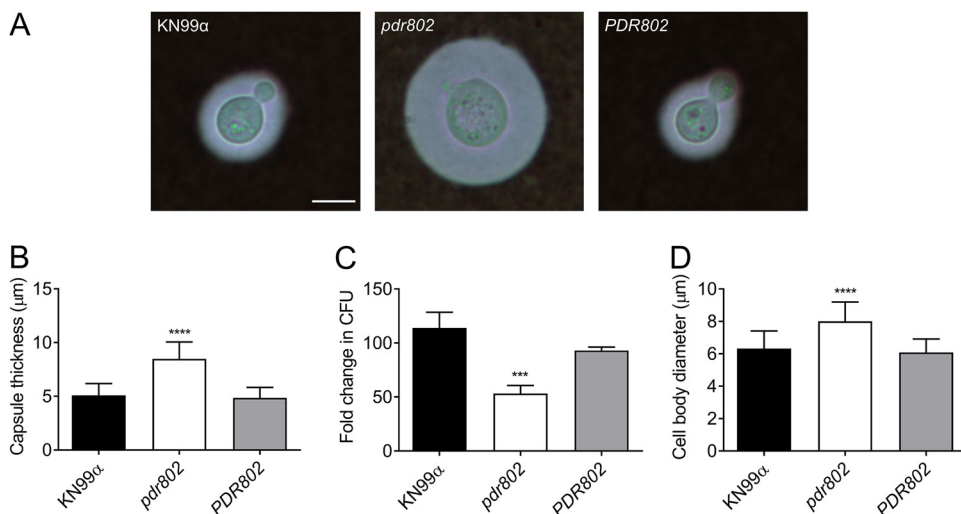
FIG 4 Growth in mouse serum elicits increased capsule thickness and cell body diameter in the *pdr802* mutant. (A) Light micrographs of the indicated strains after growth in mouse serum (at 37°C, 5% CO_2) for 24 h and negative staining with India ink to visualize the capsule. All images are to the same scale; bar, 5 μm. (B) Mean and SD of capsule thickness, assessed by measuring at least 50 cells per strain with ImageJ. (C) Cells grown as described for panel A were plated on YPD to assess CFU. Mean and SD of the fold change compared to 0 h are shown. (D) Mean and SD of cell body diameter, measured as for panel B. ***, $P < 0.001$, and ****, $P < 0.0001$, compared to KN99α by one-way ANOVA with a *post hoc* Dunnett test.

To validate the observations that we had made under standard host-like conditions based on synthetic tissue culture medium, we conducted similar studies in mouse serum at 37°C and 5% CO_2. These conditions induced an even more pronounced hypercapsular phenotype of the *pdr802* mutant (Fig. 4A and B), as well as reduced cell viability (Fig. 4C) and increased cell body diameter (Fig. 4D).

We were intrigued by the enlarged cell body and capsule of the *pdr802* mutant cells under host-like conditions *in vitro* and decided to examine these phenotypes *in vivo*. For these studies, we isolated fungal cells from the lungs of mice at various times after infection and assessed their morphology by negative staining (Fig. 5A). At each time point, the mean mutant cell body diameter was larger than that of the controls. Additionally, while this parameter was stable for WT and complemented strains throughout the infection period, it trended larger at the end of the infection period for the deletion mutant (Fig. 5B). In contrast, mutant capsule thickness, although initially greater than that of control cells, changed little throughout the period, while capsule thickness of control cells increased to that level or beyond (Fig. 5C). Furthermore, although the total diameter of *pdr802* cells consistently exceeded that of WT and complemented cells, their sizes became more comparable late in infection (Fig. S6A). Over time, therefore, the ratio of total cell diameter to cell body diameter for WT and *PDR802* cells steadily increased, while it remained roughly constant for the mutant (Fig. S6B).

Pdr802 negatively regulates Titan cell formation. We were particularly interested in the cell size phenotype of *pdr802* because Titan cells have been strongly implicated in cryptococcal pathogenesis (19). By any definition of this morphotype (cell body diameter greater than 10 or 15 μm or total cell diameter greater than 30 μm), our mutant cell populations were dramatically enriched in Titan cells at every time of infection that we assessed (Fig. S6C).

To specifically test Titan cell formation by the *pdr802* strain, we subjected mutant cells to *in vitro* conditions that induce this process (49) (Fig. 6A) and analyzed the resulting population by flow cytometry. Consistent with our *in vivo* observations, Titan cells constituted a much larger fraction of the population in the mutant culture (8.46%)
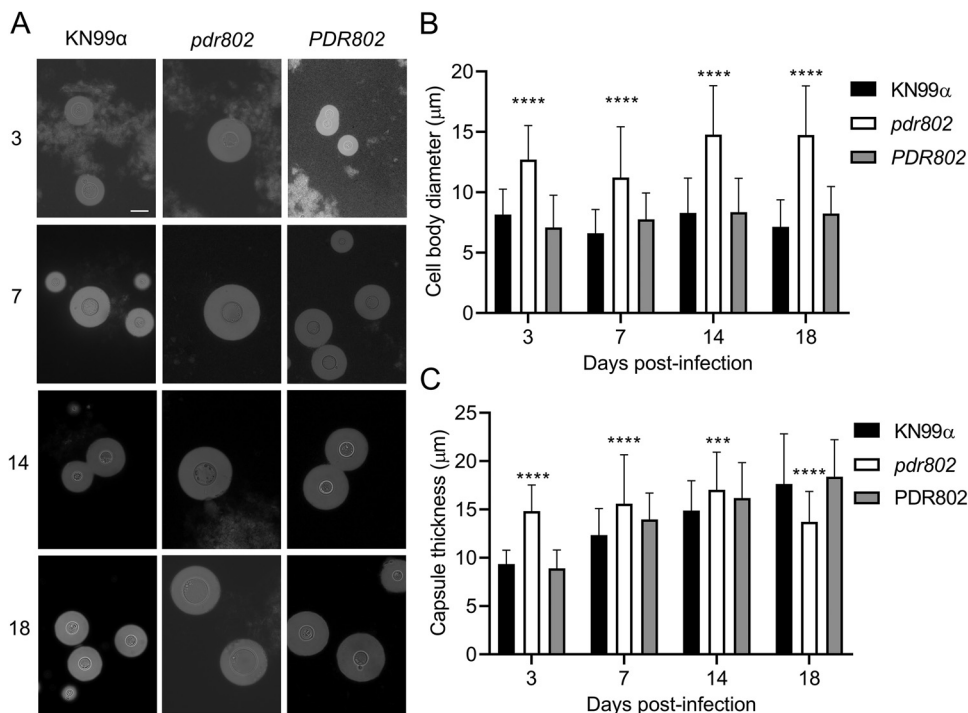
FIG 5 Absence of *PDR802* yields enlarged cells and loss of capsule induction in the context of animal infection. (A) India ink staining of fungi isolated from the lungs of mice infected with the indicated strains. Numbers at left are days post-infection. All images are to the same scale; bar, 10 μm. (B and C) Means and SD of cell body diameter (B) and capsule thickness (C), assessed by measuring at least 50 cells per strain with ImageJ. ****, $P < 0.0001$, and ***, $P < 0.001$, compared to KN99α by one-way ANOVA with a *post hoc* Dunnett test for each day post-infection.

than in the WT and complemented cultures (1.38% and 1.13%, respectively) (Fig. 6B). As expected for Titan cells, these cells are also polyploid (Fig. 6C).

Titan cells are poorly engulfed by host phagocytes (19, 45, 73), which may reflect their increased size as well as alterations in capsule and cell wall (51). We observed this reduced uptake for all strains after growth in conditions that favor Titan cell formation (Fig. 7, Titan versus YPD). Also, all strains showed a reduction in phagocytosis after capsule induction in DMEM (Fig. 7, DMEM versus YPD), which is not surprising, because the capsule is antiphagocytic (31, 73). Notably, the reduction in uptake was greatest for the *pdr802* mutant under both of these conditions, even though it showed normal engulfment when all strains were grown under control conditions (YPD). This is likely because the mutant culture is both hypercapsular and enriched in Titan cells.

Identification of direct, functional targets of Pdr802. To identify direct targets of Pdr802, we next performed chromatin immunoprecipitation followed by sequencing (ChIP-Seq). We compared DNA sequences immunoprecipitated by anti-mCherry monoclonal antibody (MAb) from cells expressing mCherry-Pdr802, which grow similarly to the WT (Fig. S7A), and untagged cells. Both strains were grown for 24 h in DMEM at 37°C and 5% CO_2, as these conditions induce *PDR802* expression dramatically compared to standard YPD growth conditions (Fig. 2).

Using 2-fold-enrichment over control as a cutoff value for peaks with adjusted P values of <0.05, we identified 656 binding sites for mCherry-Pdr802 in genomic DNA. Of these, 540 occurred within 1,000 bp upstream of transcription start sites (Data Set S1, sheets 1 and 2), which we used as an approximation of regulatory regions. Notably, ChIP-Seq data for the region upstream of the *PDR802* transcription start site suggested self-regulation, as has been reported for other cryptococcal TFs (74, 75) (Fig. S7B). We further applied discriminative regular expression motif elicitation (DREME) (76) to the
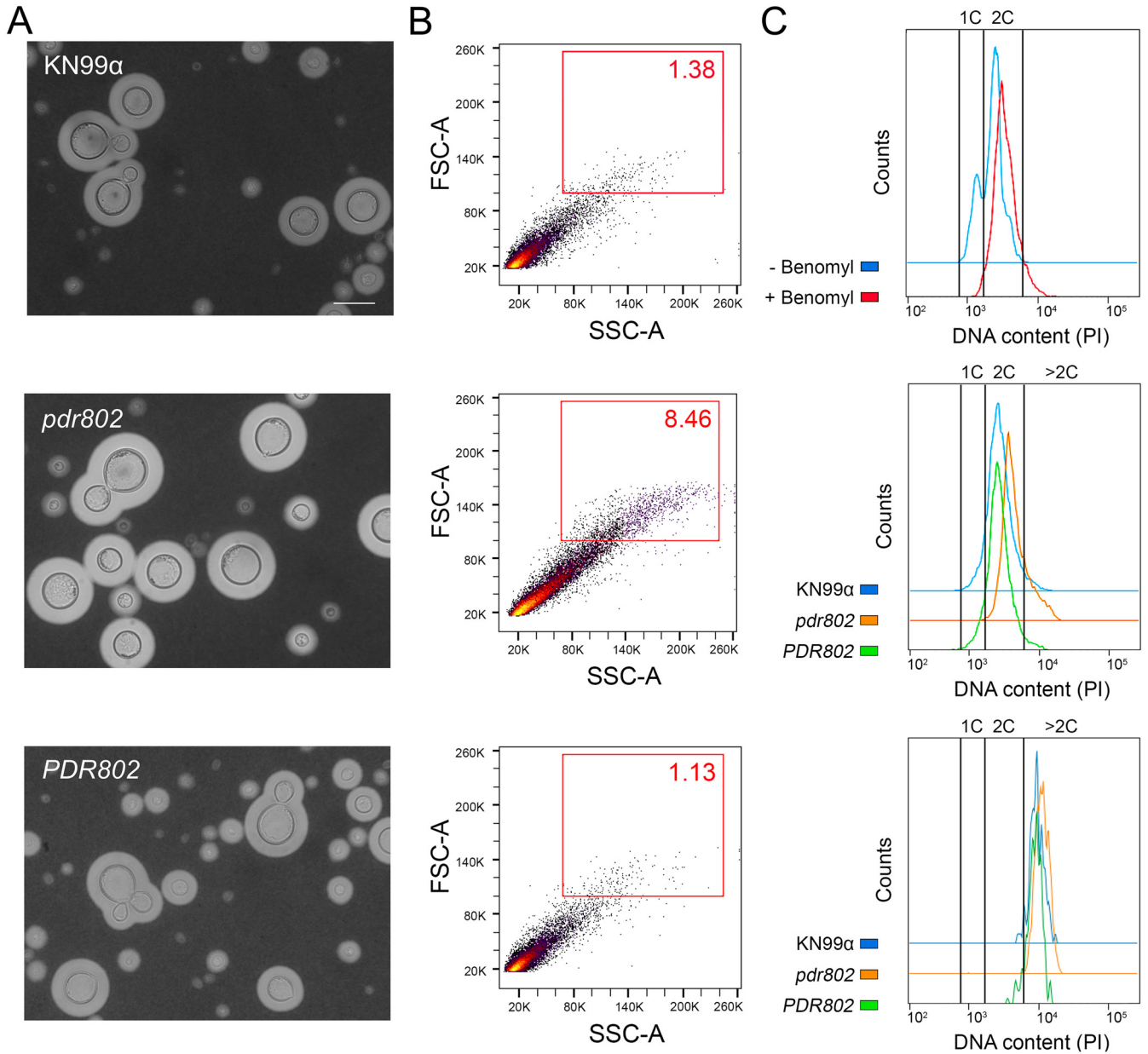
FIG 6 Pdr802 is a negative regulator of Titan cell formation. (A) The indicated strains were subjected to *in vitro* conditions that induce Titan cell formation and imaged with India Ink. All images are to the same scale; bar, 10 μm. Images were selected so that each shows multiple examples of Titan cells, not to reflect abundance of this morphotype. (B) The percentage of Titan cells in each culture was quantified using flow cytometry, gated as indicated by the red square. FSC-A, forward scatter; SSC-A, side scatter. (C) DNA content of cells after staining with propidium iodide (PI) and analysis by flow cytometry. (Top) 1C and 2C gates determined using control cultures of KN99α grown in YNB without or with benomyl, which traps cells at 2C. (Middle) Profiles of the indicated strains after growth under Titan cell-inducing conditions, showing an increased polyploid tail in mutant cultures relative to wild-type cells. (Bottom) DNA content profiles for only the Titan cells (gated as for panel B, red box) for each strain, showing their polyploid nature.

set of 540 upstream regions to identify putative Pdr802 binding motifs; these were highly enriched in GA (TC) (Fig. S7C).

To complement our ChIP studies, we determined the set of genes regulated by Pdr802 under host-like conditions by performing RNA-Seq of WT and *pdr802* cells after growth for 24 h in DMEM at 37°C and 5% CO_2 (Data Set S1, sheet 3). We then used dual-threshold optimization (DTO) to analyze the RNA-Seq and ChIP-Seq data sets together. This statistical method allowed us to combine the evidence from binding and expression studies to converge on a set of direct and functional TF targets (77); because it uses two independent lines of evidence to suggest regulatory relationships, it
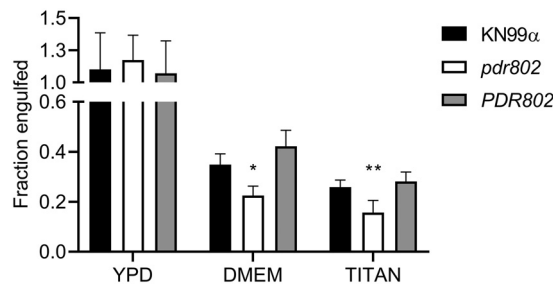
FIG 7 Deletion of *PDR802* affects phagocytosis after growth under conditions that induce capsule and Titan cell formation. *C. neoformans* strains were grown in YPD (18 h), DMEM (24 h), or Titan cell induction medium (72 h) and then incubated for 2 h with J774.16 mouse macrophages; host cells were then washed and lysed to assess fungal burden by CFU. Data shown are normalized to the CFU of the initial inoculum. *, $P < 0.05$, and **, $P < 0.01$, compared to KN99α by one-way ANOVA with a *post hoc* Dunnett test.

increases confidence in highly significant small effects. The Pdr802 target genes yielded by this analysis include key players in multiple processes implicated in cryptococcal virulence, including quorum sensing, Titan cell formation, and stress resistance (Data Set S1, sheets 4 and 5).

Pdr802 regulates the expression of quorum sensing proteins that control Titan cell formation. The most striking phenotype we observed in cells lacking *PDR802* is the marked increase in Titan cell formation. We therefore examined our DTO target list for genes known to influence this phenotype, such as those involved in quorum sensing. Recent studies have shown that the quorum sensing peptide Qsp1 is a negative regulator of Titan cell formation (47, 48); Titan cell formation increases upon deletion of the gene encoding this peptide (*QSP1*) or proteins that mediate its maturation and import (*PQP1* and *OPT1*, respectively). We found that Pdr802 positively regulates *PQP1* and *OPT1* gene expression (Table 1), consistent with its repression of Titan cell formation.

A study of *C. neoformans* cells exposed to Titan cell-inducing conditions *in vitro* reported that 562 genes were upregulated under this condition, while 421 genes were downregulated (48). The overlap of these genes with our DTO set of Pdr802-regulated genes included the TF genes *LIV3*, *STB4*, and *ZFC3* (48) (Data Set S2, sheets 1 and 2). The first two are repressed during Titan cell induction, while *ZFC3* (also known as *CQS2*) is induced. Our analysis showed that Pdr802 positively regulates expression of *LIV3* and *STB4*, while it negatively regulates *ZFC3* (Table 1), in concordance with our phenotypic observations of Titan cell formation. Notably, Liv3 and Zfc3 are responsive to the peptide Qsp1 (74, 75) and are important for *C. neoformans* virulence, while Stb4 influences cryptococcal brain infection (67).

Pdr802 coordinates cryptococcal response to the host environment. *C. neoformans* deploys a variety of proteins to resist the many challenges it experiences upon host entry, which include oxidative and temperature stress. Multiple genes that are central to these responses were identified as direct, functional targets of Pdr802 by our DTO analysis (Table 2). For example, Pdr802 induces the expression of genes whose products detoxify reactive oxygen species (ROS), such as *CAT1*, *CAT2*, and *SOD1* (78, 79), or participate in resistance to these compounds, such as *FZC34*, *MIG1*, and *CCK1* (52, 80, 81) (Table 2). Both the kinase Cck1 (also known as Yck2) and the TF Fzc34 have been implicated in cryptococcal virulence (80, 82).

As noted above, the pigment melanin has important antioxidant properties that promote cryptococcal survival inside the host (16). Under host-like conditions, Pdr802 regulates genes required for melanization, even though it melanizes normally *in vitro*. These genes include *CAC1*, *PKC1*, *CUF1*, and *SNF5* (Table 2). Cac1 is an adenylyl cyclase responsible for cyclic AMP (cAMP) production in *C. neoformans*, which plays a central role in melanin synthesis as well as proper capsule production, mating, and virulence (83). The kinase Pkc1 induces production of the laccase (Lac1) that forms melanin and

TABLE 1 Pdr802 target genes involved in quorum sensing and Titan cell formation

Biological process	CNAG ID[a]	Gene name	Change determined by:		Description
			ChIP-Seq[b]	RNA-Seq[c]	
Quorum sensing	00150	PQP1	1.38	−0.78	Peptidase
	03013	OPT1	1.25	−0.55	OPT small oligopeptide transporter
Titan cell formation	05835	LIV3	1.52	−0.84	Transcription factor
	05785	STB4	3.33	−1.71	Transcription factor
	05940	ZFC3/CQS2	2.23	0.68	Transcription factor

[a]CNAG, *Cryptococcus neoformans* serotype **A g**enome project gene identifier (118).
[b]Fold change for mCherry-Pdr802 compared to WT.
[c]Log$_2$ fold change for *pdr802* compared to WT.

plays a key role in resistance to oxidative and nitrosative stress (84, 85), the TF Cuf1 regulates *LAC1* expression and is important for cryptococcal virulence (86, 87), and *SNF5* is required for full melanization (88). Melanin occurs in the fungal cell wall, which is another key component in fungal stress resistance. Pdr802 is also a direct, functional regulator of several genes whose products influence cell wall glycan content: two chitin deacetylases (Cda3 and Mp98) and the mannoprotein MP88 (Table 2). This is also consistent with the increases in mannose and chitin that occur in Titan cell walls (51).

Pdr802 positively regulates the expression of several proteins required for yeast survival at 37°C, including the kinases Kic1 and Ire1 (Table 2). Ire1 is a regulator of the cryptococcal unfolded-protein response (UPR) pathway and lack of Ire1 or Kic1 impact *C. neoformans* virulence (80, 89). Pdr802 also modulates cryptococcal urease activity, which is required for dissemination to the central nervous system (CNS) (11, 12), by regulating the urea transporter Dur3 and other proteins that influence urease activity

TABLE 2 Genes regulated by Pdr802 involved in adaptation to the host environment

Biological process	CNAG ID[a]	Gene name	Change determined by:		Description
			ChIP-Seq[b]	RNA-Seq[c]	
Oxidative stress resistance	04981	CAT1	1.47	−1.60	Catalase 1
	05256	CAT2	1.41	−0.42	Catalase 2
	01019	SOD1	2.59	−0.53	Superoxide dismutase (Cu-Zn)
	00896	FZC34	2.22	−0.82	Transcription factor
	06327	MIG1	1.72	−0.78	DNA-binding protein CreA
	00556	CCK1	1.78	−0.48	Casein kinase I
Melanin and cell wall formation	03202	CAC1	1.60	−0.61	Adenylate cyclase
	01845	PKC1	2.00	−0.48	AGC/PKC protein kinase
	07724	CUF1	1.27	−0.67	Metal-binding regulatory protein
	00740	SNF5	1.28	−0.70	Swi/Snf chromatin-remodeling subunit
	01239	CDA3	2.63	1.08	Chitin deacetylase 3
	01230	MP98	2.74	0.96	Chitin deacetylase 2
	00776	MP88	1.86	1.23	Immunoreactive mannoprotein
Growth at 37°C	00405	KIC1	1.88	−0.97	Ste/Ste20/Ysk protein kinase
	03670	IRE1	1.66	−1.14	IRE protein kinase
Urease activity	07448	DUR3	2.13	−3.05	Urea transporter
	01209	FAB1	2.29	−0.49	1-Phosphatidylinositol-3-*P* 5-kinase
	01938	KIN1	1.61	−0.34	CAMK/CAMKL/KIN1 protein kinase
	01155	GUT1	2.96	0.62	Glycerol kinase
	00791	HLH1	1.71	−1.09	Transcription factor
Capsule thickness	02802	ARG2	1.56	−0.59	Inositol/phosphatidylinositol kinase
	06809	IKS1	2.28	−0.44	IKS protein kinase
	01905	KSP1	2.02	−0.64	Serine/threonine protein kinase
	02877	FZC51	1.75	−0.69	Transcription factor
	07470	PDE2	2.42	−1.80	High-affinity phosphodiesterase
	03346	BZP4	3.52	1.30	Transcription factor
Calcineurin signaling	00156	CRZ1	1.44	−0.49	Transcription factor
	01744	HAD1	2.26	0.47	Phosphatase

[a]CNAG, *Cryptococcus neoformans* serotype **A g**enome project gene identifier (118).
[b]Fold change for mCherry-Pdr802 compared to WT.
[c]Log$_2$ fold change for *pdr802* compared to WT.
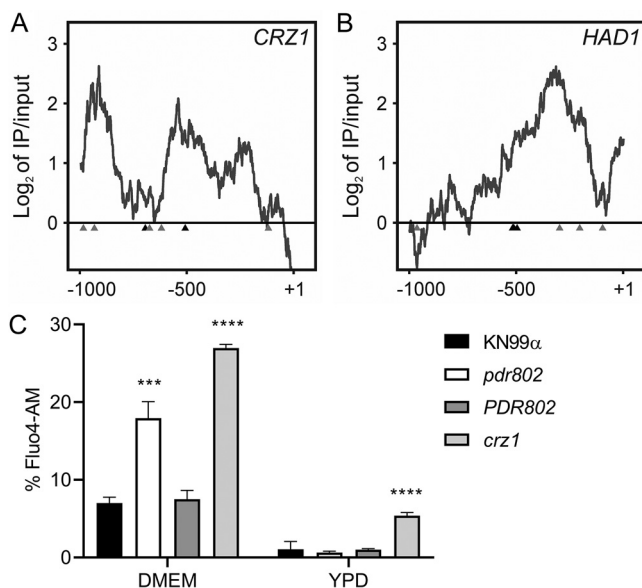
FIG 8 Pdr802 participates in calcineurin signaling. (A and B) Interactions of Pdr802 with upstream regions of the indicated genes. The ratios (log$_2$) of reads from immunoprecipitated (IP) DNA to input DNA were calculated for 1,000 bp upstream of the first coding nucleotide (+1); shown is the difference in these values between tagged and untagged strains. Black triangles, complete Pdr802 DNA-binding motifs (Fig. S7C); gray triangles, partial motifs. (C) Intracellular calcium measurement by flow cytometry using Fluo-4AM. Each column shows the mean and standard deviation of three biological replicates. ***, $P < 0.001$, and ****, $P < 0.0001$, compared to KN99α by one-way ANOVA with a *post hoc* Dunnett test.

(e.g., the kinases Fab1, Kin1, and Gut1 and the TF Hlh1) (Table 2). Deletion of *FAB1*, *KIN1*, or *HLH1* impaired urease activity in *C. neoformans*, while *GUT1* disruption induced it (52, 80).

Above, we document the role of Pdr802 in capsule synthesis, which is dramatically upregulated in the host environment in general and is further increased in cells lacking this TF. We found that Pdr802 is a positive regulator of multiple genes that have been implicated in reducing cryptococcal capsule thickness. These include the kinases Arg2, Iks1, and Ksp1; the TF Fzc51; and the phosphodiesterase Pde2 (Table 2). Notably, null mutants for those genes are hypercapsular, similar to *pdr802* cells (52, 80, 90). Pdr802 is a negative regulator of the TF Bzp4, which, as mentioned above, positively regulates capsule (Table 2) (52).

Pdr802 regulates calcineurin target genes. The calcineurin signaling pathway is activated by calcium and governs stress response and virulence in *C. neoformans* (91–93). One major mediator of calcineurin signaling is the transcription factor Crz1 mentioned above, which is highly responsive to temperature and influences cryptococcal virulence (57, 62). Upon intracellular calcium influx, calcineurin dephosphorylates Crz1, which then translocates to the nucleus and regulates gene expression (57, 63). We found that Pdr802 binds the *CRZ1* gene promoter and positively regulates its expression (Fig. 8A, Table 2, and Data Set S2, sheet 3). Pdr802 also binds and regulates five other genes whose products are dephosphorylated by calcineurin; these include the phosphatase Had1, which is important for cryptococcal cell wall remodeling and virulence (Fig. 8B, Table 2, and Data Set S2, sheet 3) (63, 94).

Because Crz1 helps maintain normal cryptococcal Ca^{2+} concentrations through the regulation of calcium transporters (57), we wondered about the intracellular calcium levels in *pdr802* cells. We found that indeed, after 24 h of growth in DMEM, the level of cytosolic calcium in the mutant significantly exceeded that of WT or complemented strains (Fig. 8C). It was still, however, below that of a *crz1*-null mutant, supporting the idea that Pdr802 is not the sole regulator of *CRZ1* expression. Notably, *PDR802* deletion

had no effect in rich medium (YPD), which reinforces our hypothesis that Pdr802 acts primarily under host-like conditions. To further explore the relationship of Pdr802 and calcineurin, we compared published gene expression profiles of a calcineurin mutant (57) to our DTO data set. Of the 393 genes that are differently expressed in the calcineurin mutant under thermal stress, 26 are regulated by Pdr802 (Data Set S2, sheet 4).

DISCUSSION

We have shown that Pdr802 is a potent regulator of cryptococcal responses to the host environment. In this context, it influences the formation of capsule and Titan cells as well as cellular responses to temperature and oxidative stress, acts as a downstream effector of calcineurin, and modulates calcium availability. The last function is likely achieved through its positive regulation of the transcription factor Crz1, which in turn modulates the calcium transporters Pmc1 and Vcx1 (57). Since calcium ion is a major second messenger in eukaryotic cells, its accumulation in *pdr802* cells affects multiple processes central to host interactions, including stress responses, cell wall integrity, and capsule size (61, 62, 92, 95, 96).

C. neoformans dissemination to the brain is the main driver of patient mortality (2). We found that dissemination of *pdr802* cells is significantly impaired, although they do occasionally reach the brain. These observations can be explained by a combination of factors. First, the limited accumulation of the *pdr802* mutant in the lungs, due to factors summarized above, may directly affect dissemination (97). Second, this strain survives poorly in mouse serum, as demonstrated directly by our culture experiments and indirectly by our inability to detect it in the blood of infected mice, even 75 days after infection. The latter might occur because the cells do not reach the blood or because they are rapidly eliminated, consistent with previous observations (98). Third, the thick capsules of the *pdr802* mutant reduce its ability to reach the brain. This is true whether fungal entry occurs directly, by the movement of free fungi across the BBB, or indirectly, via a Trojan horse mechanism that requires macrophage uptake (99); such uptake is impeded by enlarged capsules, independent of cell size (31). Fourth, calcium imbalance directly affects cryptococcal transmigration (100). Finally, *pdr802* cells show reduced expression of genes required for urease activity, which promotes *C. neoformans* dissemination to the CNS (11, 12, 100). Interestingly, despite all of these obstacles to dissemination, mutant cells that do reach the brain are able to proliferate to wild-type levels.

Titan cells are a robust and persistent morphotype of *C. neoformans* that contribute to yeast virulence (45). We showed that cells lacking Pdr802 demonstrate increased formation of Titan cells *in vivo* and *in vitro*, suggesting that this TF is a novel repressor of this process. Although Titan cells enhance aspects of cryptococcal pathogenesis (19, 101), their overproduction negatively impacts dissemination to the brain due to their resistance to phagocytosis by macrophages (19, 45) and decreased penetration of biological barriers (19).

Our combined analysis of DNA binding and gene expression data allows us to understand the increase in Titan cell formation that occurs upon deletion of *PDR802*. Under host-like conditions, Pdr802 positively regulates Pqp1, Opt1, and Liv3, all key proteins in the cryptococcal quorum sensing pathway, which represses Titan cell formation (47, 48). In the absence of this TF, quorum sensing is impaired, a situation known to increase Titan cell formation. Pdr802 may also indirectly regulate Titan cell formation by regulating other TFs that impact this process, such as Zfc3 (Cqs2) and Stb4.

We know that capsule, a key virulence factor, is typically highly induced in the host or under host-like conditions (102). Our studies *in vitro*, *ex vivo*, and *in vivo* show that Pdr802 normally reins in this process. This likely occurs via a combination of Pdr802's repression of the TF Bzp4, which positively regulates capsule size, and the induction of other factors (e.g., the TF Fzc1, the phosphodiesterase Pde2, and the kinases Ksp1, Arg2, and Iks1) that negatively regulate capsule size (52, 80, 90).

Overall, we found that Pdr802 influences key cryptococcal phenotypes that

influence virulence, including quorum sensing, stress responses, Titan cell formation, and capsule production (Fig. 9). We have further identified multiple genes that are central in these processes and are directly regulated by Pdr802. Some of these targets are also regulated by calcineurin (e.g., Had1 and Crz1) or by another important TF, Gat201 (e.g., Opt1, Liv3, and Zfc3) (60, 74, 75). Finally, the expression of *PDR802* itself is regulated by the TFs Gat201 and Hob1 (67, 75). The cross talk between all of these regulatory mechanisms remains to be dissected. Nonetheless, it is evident that Pdr802 is critical for both survival in the lung and dissemination to the brain, thus explaining its role in cryptococcal virulence.

MATERIALS AND METHODS

Strain construction and cell growth. We previously reported the *PDR802* deletion mutant (*pdr802*) in the KN99α strain background (103) that was used in this work (39). Complementation of this mutant with the wild-type gene at the native locus (*PDR802*) and construction of a strain that expresses Pdr802 with N-terminal mCherry (mCherry-Pdr802) are detailed in the supplemental methods. For all studies, *C. neoformans* strains were inoculated from single colonies into YPD medium (2% [wt/vol] dextrose, 2% [wt/vol] Bacto peptone, and 1% [wt/vol] yeast extract in double-distilled water [ddH$_2$O]) and grown overnight at 30°C with shaking at 230 rpm before further handling as detailed below. To assess viability during growth in tissue culture medium, overnight cultures were washed with phosphate-buffered saline (PBS), diluted to 10^6 cells/ml in DMEM (Sigma; D6429), plated (1 ml/well) in triplicate in 24-well plates, and incubated at 37°C and 5% CO$_2$. At the indicated times, cells were mixed thoroughly, diluted in PBS, and plated on YPD agar (YPD medium, 2% agar [wt/vol]) for assessment of CFU. To assess viability during growth in mouse serum, mouse blood was collected as described below in "Animal experiments"; YPD-grown cryptococcal cells were incubated in 100 μl of serum in 96-well plates for 24 h at 37°C and 5% CO$_2$, and CFU were counted as described above.

Animal experiments. All animal protocols were approved by the Washington University Institutional Animal Care and Use Committee (reference 20170131) or Comissão de Ética no Uso de Animais (CEUA) (reference 30936), and care was taken to minimize handling and discomfort. For survival studies, groups of five 4- to 6-week-old female C57BL/6 mice (The Jackson Laboratory) were anesthetized by subcutaneous injection of 1.20 mg ketamine and 0.24 mg xylazine in 120 μl sterile water and intranasally infected with 5×10^4 cryptococcal cells. The mice were monitored and humanely sacrificed when their weight decreased to below 80% of initial weight or if they showed signs of disease, at which point organ burden was assessed. The lungs and brains were harvested, homogenized, diluted, and plated on YPD agar. The resulting CFU were enumerated, and survival differences were assessed by Kaplan-Meier analysis.

For timed organ burden studies, *C. neoformans* overnight cultures were centrifuged (1,000 × *g* for 3 min), washed with sterile PBS, and resuspended in PBS to 1×10^6 cells/ml. Groups of three 4- to 6-week-old female C57BL/6 mice (Centro Multidisciplinar para Investigação Biológica na Área da Ciência em Animais de Laboratório [CEMIB]) were anesthetized as described above, intranasally infected with 5×10^4 cryptococcal cells, and monitored as described above. At set time points post-infection (see above), mice were sacrificed and fungal burden was assessed from organs (as described above) or blood (obtained by cardiac puncture). Organ burden was analyzed by Kruskal-Wallis test with Dunn's multiple comparison *post hoc* test for each day post-infection.

To assess cryptococcal viability in mouse serum, 6 BALB/c mice were anesthetized with isoflurane and blood was collected from the retro-orbital space using a sterile capillary tube. Collected blood was incubated at 37°C for 30 min, and serum was isolated by centrifugation at 1,000 × *g* for 15 min and then heat inactivated at 56°C for 30 min.

Capsule analysis. To qualitatively assess capsule thickness, strains were grown on YPD medium for 16 h and washed with PBS, and 10^3 cells were incubated in mouse serum for 24 h at 37°C and 5% CO$_2$. After incubation, cells were fixed in 4% paraformaldehyde and washed three times with PBS. *C. neoformans* cells were placed on glass slides and mixed with similar volumes of India ink, and the capsule was measured as previously described (104).

For population-level capsule measurement, *C. neoformans* strains were grown overnight in YPD, washed with PBS, and diluted to 10^6 cells/ml in DMEM. Aliquots (150 μl) were then plated in quadruplicate in the middle 32 wells of a poly-L-lysine-coated 96-well plate (Fisher; 655936) and incubated at 37°C and 5% CO$_2$. After 24 h, the cells were washed with PBS and incubated with 150 μl of a staining mixture (100 μg/ml calcofluor white to stain cell walls, 50 μg/ml of the anticapsular monoclonal antibody 302 conjugated to Alexa Fluor 488 [Molecular Probes], and 1.5% goat serum in PBS) for 30 min at room temperature in the dark. The cells were washed again with PBS, fixed with 4% formaldehyde for 10 min at room temperature, and washed with PBS, and each well was refilled with 150 μl PBS. The cells were imaged using a BioTek Cytation 3 imager, which automatically collected 100 images per well in a grid pattern at the well center. Image files were prepared for analysis with GE Healthcare IN Cell Translator and assembled into .xdce image stacks for analysis with GE Healthcare IN Cell Developer Toolbox 1.9. Cell wall and capsule images were first filtered to remove background noise and border objects, and then cells were identified using shape-based object segmentation (3-pixel kernel, 50% sensitivity) followed by watershed clump breaking to prevent apparent connectivity caused by incomplete segmentation. Target linking was performed to assign each cell wall object to one capsule object based on known 1:1 pairing and location, generating a target set. Capsule and cell wall object diameters were calculated
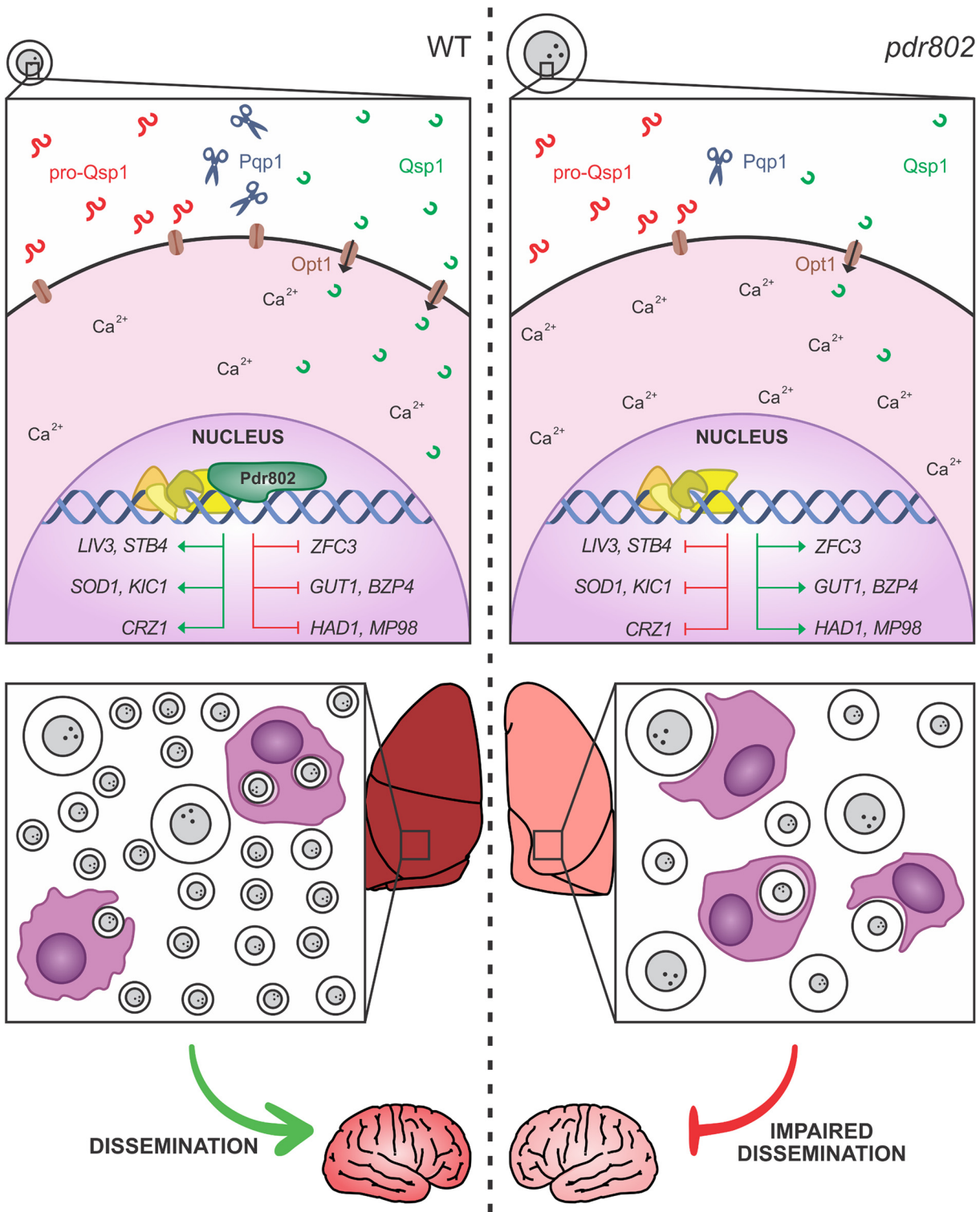
FIG 9 Pdr802 mode of action. (Left) When wild-type *C. neoformans* enters a host, *PDR802* expression is induced and Pdr802 positively regulates elements of the quorum sensing pathway (described in the text) as well as expression of TFs implicated in this pathway (*LIV3*), Titan cell production (*ZFC3*), and brain infectivity (*STB4*). At the same time, Pdr802 regulates two calcineurin targets (*CRZ1* and *HAD1*) and a variety of other genes (see the text). Shown are a few examples of genes involved in the response to oxidative stress (*SOD1*), growth at 37°C (*KIC1*), urease activity (*GUT1*), capsule production (*BZP4*), and cell wall remodeling (*MP98*). (Right) In the absence of these regulatory changes, *pdr802* cells are poorly equipped to survive the stress of the host environment and are subject to increased intracellular calcium levels, dysregulation of capsule production, and impaired stress resistance. As a result, the cryptococcal population in the lung is smaller and is enriched in Titan cells and hypercapsular cells of normal size, both of which demonstrate reduced phagocytosis by host cells and impaired ability to cross biological barriers; these defects reduce dissemination to the central nervous system.

for each target set (hundreds to thousands per well), and the difference between measurements in each pair was defined as the capsule thickness. Data were normalized by the difference in capsule thickness between uninduced and induced WT cells, which were included in each experiment, and compared to data for hypercapsular (*pkr1*) (39) and hypocapsular (*ada2*) (105) control strains in each experiment. Capsule sizes were compared by one-way analysis of variance (ANOVA) with Dunnett's multiple compari-son *post hoc* test.

To measure capsule thickness of cryptococcal cells grown in the lungs of infected mice, lung homog-enates were filtered through a cell strainer with 40-μm pores using a syringe plunger, fixed in 3.7% formaldehyde, and used for India ink staining and measurement as described above. For the visualiza-tion of KN99α and *PDR802* cells from mouse lungs after 18 days of infection, the tissue was treated with 50 μg/ml DNase I for 30 min at 37°C.

GXM immunoblotting was conducted as previously described (71). Briefly, 10^6 cells/ml were grown in DMEM for 24 and 48 h. Culture supernatant fractions were then resolved by gel electrophoresis on 0.6% agarose, transferred onto nylon membranes, and probed with 1 μg/ml anti-GXM antibody 302.

Phenotypic assays. For stress plates, cryptococcal cells were grown overnight in YPD, washed with PBS, and diluted to 10^7 cells/ml in PBS. Aliquots (3 μl) of 10-fold serial dilutions were spotted on YPD or YNB agar supplemented with various stressors (sorbitol, NaCl, CaCl$_2$, LiCl, Congo red, calcofluor white, caffeine, SDS, NaNO$_2$, H$_2$O$_2$, and ethanol) at the concentrations indicated in the figures. Melanization was tested on plates made by mixing 10 ml of 2× minimal medium (2 g/liter L-asparagine, 1 g/liter MgSO$_4$ s^2 7H$_2$O, 6 g/liter KH$_2$PO$_4$, 2 g/liter thiamine, 2 mM L-3,4-dihydroxyphenylalanine [L-DOPA]; 0.1% dextrose was added for melanization induction, and 0.5% was added for melanization inhibition) with 10 ml of 2% agar-water per plate. A control strain lacking the ability to melanize was used as a control (*lac1*) (88). For the solid urease assay, 10 μl of a 10^7 cells/ml suspension in water was plated on Christensen's urea solid medium (1 g/liter peptone, 1 g/liter dextrose, 5 g/liter NaCl, 0.8 g/liter KH$_2$PO$_4$, 1.2 g/liter Na$_2$HPO$_4$, 0.012 g/liter phenol red and 15 g/liter agar; pH 6.8). Plates were incubated at 30°C or 37°C.

Titan cells. Titan cell induction was performed in 1× PBS supplemented with 10% heat-inactivated fetal calf serum (FCS) for 72 h at 37°C and 5% CO$_2$ as recently described (49) and quantified by flow cytometry as previously reported (47, 48). For analysis of DNA content, cells were treated as previously described (47) with a few modifications. Briefly, cultures were fixed with 70% ethanol for 1 h at 24°C and then overnight at 4°C, washed twice with PBS, and then treated with propidium iodide (50 μg/ml) and RNase A (0.5 mg/ml) in PBS for 2 h at 30°C with agitation. Quantification was performed using a FACS ARIA III (BD) cytometer with analysis on the Cytobank platform. A total of 20,000 events were recorded, and doublets were filtered out using comparisons of forward-scatter width (FSC-W) versus forward-scat-ter height (FSC-H) to exclude events with high FSC-W and FSC-H. To define the 1C and 2C gates, cells were grown in yeast nitrogen base (YNB) (24 h, 30°C, 150 rpm) without or with 80 μg/ml benomyl, which traps cells in 2C, as recently reported (106).

Phagocytosis. J774.16 cells were prepared for uptake experiments by seeding (10^5 cells/well) in a 96-well plate and incubating in DMEM supplemented with 10% fetal bovine serum (FBS) at 37°C and 5% CO$_2$ for 24 h. *C. neoformans* cells were prepared for uptake experiments by inoculating an overnight cul-ture in YPD into either DMEM or Titan cell induction medium (49) and growing at 37°C and 5% CO$_2$ for 24 or 72 h, respectively. To initiate the study, cryptococcal cells were washed with PBS and opsonized with anti-capsular antibody 18B7 (1 μg/ml) for 1 h at 37°C, while macrophages were activated with 50 nM phorbol myristate acetate (PMA) for 1 h at 37°C and 5% CO$_2$; 10^6 cryptococcal cells were then incubated with the macrophages for 2 h at 37°C and 5% CO$_2$. The wells were then washed three times with warm PBS, and the macrophages were lysed with 0.1% Triton in PBS and plated for CFU enumera-tion as described above. Fold change in numbers of CFU was assessed by comparison to the CFU of opsonized cells. One-way ANOVA with Dunnett's multiple-comparison *post hoc* test was used to com-pare phagocytosis of *pdr802* and *PDR802* strains with that of KN99α.

Chromatin immunoprecipitation. ChIP studies were performed as previously described (39, 105). Briefly, wild type and N-terminal-mCherry-Pdr802 strains were cultivated in DMEM for 24 h at 37°C and 5% CO$_2$. The cells were then fixed with formaldehyde and lysed by mechanical bead-beating, and the cell debris was removed by centrifugation. The supernatant fraction was sheared by sonication and cen-trifuged, and an aliquot was reserved as "input." The remaining material was incubated with rabbit IgG anti-mCherry antibody (Abcam; ab213511) tethered to protein A Sepharose (IP) or Sepharose alone over-night at 4°C. The beads were then washed, incubated at 65°C to reverse DNA-DNA and DNA-protein cross-links, and the DNA was recovered by phenol-chloroform-isoamyl alcohol (25:24:1) extraction, etha-nol precipitation, and resuspension in nuclease-free water.

Samples were submitted to the Washington University Genome Technology Access Center for library preparation, and DNA samples were sequenced using the Illumina NextSeq platform. The first replicate was sequenced using paired-end 2 × 75-bp reads, and replicates 2 and 3 were sequenced using single-end 75-bp reads; the minimum coverage obtained was ~16×. The quality of the reads was evaluated by FastQC (107). Fastq files were aligned to the KN99 genome (108) using NextGenMap 0.5.3 (109). SAM files were converted to bam, reads were sorted and indexed, and read duplicates were removed from the final bam files using SAMtools (110). SAMtools was also used to filter out reads with a mapping qual-ity of less than 20 phreds to guarantee single alignment of the reads. Peaks were called using MACS2 (2.1.1.20160309) (111), filtered by size (maximum threshold of 5 kb and no minimum), and annotated using Homer 4.8 (112). The significant peaks were chosen using the cutoff of fold enrichment above 2 and an adjusted *P* value of <0.05, and read coverage of each peak was obtained using SAMtools (110). Pdr802 binding motifs were identified using DREME (76); partial motifs were defined as at least 5 consec-utive base pairs of the motif.

RNA-Seq and DTO. RNA from wild-type and *pdr802* cells grown for 24 h in DMEM (37°C, 5% CO_2) was isolated and sequenced as previously described (39). Briefly, cDNA samples were sequenced using the Illumina NextSeq platform for paired-end 2×75 bp reads and read quality was evaluated by FastQC (107). Fastq files were aligned to the KN99 genome (108) using NovoAlign (113), SAM files were converted to bam, reads were sorted and indexed, and read duplicates were removed from the final bam files using SAMtools (110). The number of reads mapped per gene was calculated using HTSeq (114), and differential gene expression was analyzed with DESeq2 (115), using the independent hypothesis weighting (IHW) package to calculate the adjusted P values (116). Dual-threshold optimization (DTO) analysis was performed as recently described (77). This is a method for simultaneously finding the best thresholds for significance in a TF binding location data set (e.g., ChIP) and a TF perturbation response data set (e.g., RNA-Seq of a TF mutant). It works by trying out all pairs of thresholds for the two data sets, picking the pair that minimizes the probability of the overlap between the bound and responsive gene sets occurring by chance under a null model, and testing the significance of the overlap by comparison to randomly permuted data. Our application of DTO to our ChIP and RNA-Seq data yielded 1,455 bound genes, 5,186 responsive genes, and 1,167 genes that were both bound and responsive. Based on DTO, Pdr802 has an acceptable convergence from binding and perturbation, with a P value of <0.01 from the random permutation test and minimum expected false discovery rate (FDR) less than or equal to 20% at 80% sensitivity. In addition to requiring a statistically significant overlap between the ChIP-Seq and RNA-Seq gene sets, we filtered out any genes for which traditional differential expression analysis yielded an adjusted P value of ≤ 0.15 or absolute fold change of ≥ 0.3, leaving 380 bound targets.

Intracellular calcium measurement. To measure intracellular free Ca^{2+}, yeast cells were cultured overnight in YPD at 30°C with shaking, washed three times with deionized water, diluted to 10^6 cells/ml in DMEM (Sigma; D6429), plated (1 ml/well) in triplicate in 24-well plates, and incubated at 37°C and 5% CO_2 for 24 h. At the indicated times, cells were mixed thoroughly, diluted in PBS containing 2μM Fluo4-AM (Thermo Fisher), incubated at 30°C for 30 min, and analyzed using flow cytometry. The overnight culture was used as a control and treated as above.

Data availability. ChIP-Seq and RNA-Seq data files are available at the NCBI Gene Expression Omnibus under accession numbers GSE153134 and GSE162851, respectively.

SUPPLEMENTAL MATERIAL

Supplemental material is available online only.

DATA SET S1, XLSX file, 2.5 MB.
DATA SET S2, XLSX file, 0.02 MB.
TEXT S1, PDF file, 0.04 MB.
FIG S1, PDF file, 0.5 MB.
FIG S2, PDF file, 0.9 MB.
FIG S3, PDF file, 0.8 MB.
FIG S4, PDF file, 0.6 MB.
FIG S5, PDF file, 0.7 MB.
FIG S6, PDF file, 0.7 MB.
FIG S7, PDF file, 1 MB.

REFERENCES

1. Kwon-Chung KJ, Fraser JA, Doering TL, Wang ZA, Janbon G, Idnurm A, Bahn YS. 2014. *Cryptococcus neoformans* and *Cryptococcus gattii*, the etiologic agents of cryptococcosis. Cold Spring Harb Perspect Med 4: a019760. https://doi.org/10.1101/cshperspect.a019760.

2. Rajasingham R, Smith RM, Park BJ, Jarvis JN, Govender NP, Chiller TM, Denning DW, Loyse A, Boulware DR. 2017. Global burden of disease of HIV-associated cryptococcal meningitis: an updated analysis. Lancet Infect Dis 17:873–881. https://doi.org/10.1016/S1473-3099(17)30243-8.

3. Ballou ER, Johnston SA. 2017. The cause and effect of *Cryptococcus* interactions with the host. Curr Opin Microbiol 40:88–94. https://doi.org/10.1016/j.mib.2017.10.012.

4. Sabiiti W, May RC. 2012. Mechanisms of infection by the human fungal pathogen *Cryptococcus neoformans*. Future Microbiol 7:1297–1313. https://doi.org/10.2217/fmb.12.102.

5. Garcia-Hermoso D, Janbon G, Dromer F. 1999. Epidemiological evidence for dormant *Cryptococcus neoformans* Infection. J Clin Microbiol 37:3204–3209. https://doi.org/10.1128/JCM.37.10.3204-3209.1999.

6. Chang YC, Stins MF, McCaffery MJ, Miller GF, Pare DR, Dam T, Paul-Satyaseela M, Kim KS, Kwon-Chung KJ, Paul-Satyasee M. 2004. Cryptococcal yeast cells invade the central nervous system via transcellular penetration of the blood-brain barrier. Infect Immun 72:4985–4995. https://doi.org/10.1128/IAI.72.9.4985-4995.2004.

7. Huang S-H, Long M, Wu C-H, Kwon-Chung KJ, Chang YC, Chi F, Lee S, Jong A. 2011. Invasion of *Cryptococcus neoformans* into human brain microvascular endothelial cells is mediated through the lipid rafts-endocytic pathway via the dual specificity tyrosine phosphorylation-regulated kinase 3 (DYRK3). J Biol Chem 286:34761–34769. https://doi.org/10.1074/jbc.M111.219378.

8. Jong A, Wu C-H, Shackleford GM, Kwon-Chung KJ, Chang YC, Chen H-M, Ouyang Y, Huang S-H. 2008. Involvement of human CD44 during *Cryptococcus neoformans* infection of brain microvascular endothelial cells. Cell Microbiol 10:1313–1326. https://doi.org/10.1111/j.1462-5822.2008.01128.x.

9. Maruvada R, Zhu L, Pearce D, Zheng Y, Perfect J, Kwon-Chung KJ, Kim KS. 2012. *Cryptococcus neoformans* phospholipase B1 activates host cell Rac1 for traversal across the blood-brain barrier. Cell Microbiol 14:1544–1553. https://doi.org/10.1111/j.1462-5822.2012.01819.x.

10. Chen SHM, Stins MF, Huang S-H, Chen YH, Kwon-Chung KJ, Chang Y, Kim KS, Suzuki K, Jong AY. 2003. *Cryptococcus neoformans* induces alterations in the cytoskeleton of human brain microvascular endothelial cells. J Med Microbiol 52:961–970. https://doi.org/10.1099/jmm.0.05230-0.

11. Olszewski MA, Noverr MC, Chen G-H, Toews GB, Cox GM, Perfect JR, Huffnagle GB. 2004. Urease expression by *Cryptococcus neoformans* promotes microvascular sequestration, thereby enhancing central nervous system invasion. Am J Pathol 164:1761–1771. https://doi.org/10.1016/S0002-9440(10)63734-0.

12. Shi M, Li SS, Zheng C, Jones GJ, Kim KS, Zhou H, Kubes P, Mody CH. 2010. Real-time imaging of trapping and urease-dependent transmigration of *Cryptococcus neoformans* in mouse brain. J Clin Invest 120:1683–1693. https://doi.org/10.1172/JCI41963.

13. Santiago-Tirado FH, Onken MD, Cooper JA, Klein RS, Doering TL. 2017. Trojan horse transit contributes to blood-brain barrier crossing of a eukaryotic pathogen. mBio 8:e02183-16. https://doi.org/10.1128/mBio.02183-16.

14. Jarvis JN, Bicanic T, Loyse A, Namarika D, Jackson A, Nussbaum JC, Longley N, Muzoora C, Phulusa J, Taseera K, Kanyembe C, Wilson D, Hosseinipour MC, Brouwer AE, Limmathurotsakul D, White N, van der Horst C, Wood R, Meintjes G, Bradley J, Jaffar S, Harrison T. 2014. Determinants of mortality in a combined cohort of 501 patients with HIV-associated cryptococcal meningitis: implications for improving outcomes. Clin Infect Dis 58:736–745. https://doi.org/10.1093/cid/cit794.

15. Perfect JR, Dismukes WE, Dromer F, Goldman DL, Graybill JR, Hamill RJ, Harrison TS, Larsen RA, Lortholary O, Nguyen M-H, Pappas PG, Powderly WG, Singh N, Sobel JD, Sorrell TC, TCS. 2010. Clinical practice guidelines for the management of cryptococcal disease: 2010 update by the Infectious Diseases Society of America. Clin Infect Dis 50:291–322. https://doi.org/10.1086/649858.

16. Nosanchuk JD, Casadevall A. 2003. The contribution of melanin to microbial pathogenesis. Cell Microbiol 5:203–223. https://doi.org/10.1046/j.1462-5814.2003.00268.x.

17. Singh A, Panting RJ, Varma A, Saijo T, Waldron KJ, Jong A, Ngamskulrungroj P, Chang YC, Rutherford JC, Kwon-Chung KJ. 2013. Factors required for activation of urease as a virulence determinant in *Cryptococcus neoformans*. mBio 4: e00220-13. https://doi.org/10.1128/mBio.00220-13.

18. Chang YC, Kwon-Chung KJ. 1994. Complementation of a capsule-deficient mutation of *Cryptococcus neoformans* restores its virulence. Mol Cell Biol 14:4912–4919. https://doi.org/10.1128/mcb.14.7.4912.

19. Okagaki LH, Strain AK, Nielsen JN, Charlier C, Baltes NJ, Chrétien F, Heitman J, Dromer F, Nielsen K. 2010. Cryptococcal cell morphology affects host cell interactions and pathogenicity. PLoS Pathog 6: e1000953. https://doi.org/10.1371/journal.ppat.1000953.

20. Zaragoza O, Nielsen K. 2013. Titan cells in *Cryptococcus neoformans*: cells with a giant impact. Curr Opin Microbiol 16:409–413. https://doi.org/10.1016/j.mib.2013.03.006.

21. Wang Y, Aisen P, Casadevall A. 1995. *Cryptococcus neoformans* melanin and virulence: mechanism of action. Infect Immun 63:3131–3136. https://doi.org/10.1128/IAI.63.8.3131-3136.1995.

22. Mednick AJ, Nosanchuk JD, Casadevall A. 2005. Melanization of *Cryptococcus neoformans* affects lung inflammatory responses during cryptococcal infection. Infect Immun 73:2012–2019. https://doi.org/10.1128/IAI.73.4.2012-2019.2005.

23. Wang Y, Casadevall A. 1994. Susceptibility of melanized and nonmelanized *Cryptococcus neoformans* to nitrogen- and oxygen-derived oxidants. Infect Immun 62:3004–3007. https://doi.org/10.1128/IAI.62.7.3004-3007.1994.

24. Doering TL, Nosanchuk JD, Roberts WK, Casadevall A. 1999. Melanin as a potential cryptococcal defence against microbicidal proteins. Med Mycol 37:175–181. https://doi.org/10.1046/j.1365-280X.1999.00218.x.

25. Agustinho DP, Nosanchuk JD. 2017. Functions of fungal melanins: reference module in life sciences. Elsevier, New York, NY.

26. Cox GM, Mukherjee J, Cole GT, Casadevall A, Perfect JR. 2000. Urease as a virulence factor in experimental cryptococcosis. Infect Immun 68:443–448. https://doi.org/10.1128/iai.68.2.443-448.2000.

27. Bose I, Reese AJ, Ory JJ, Janbon G, Doering TL. 2003. A yeast under cover: the capsule of *Cryptococcus neoformans*. Eukaryot Cell 2:655–663. https://doi.org/10.1128/ec.2.4.655-663.2003.

28. Wang ZA, Li LX, Doering TL. 2018. Unraveling synthesis of the cryptococcal cell wall and capsule. Glycobiology 28:719–730. https://doi.org/10.1093/glycob/cwy030.

29. Agustinho DP, Miller LC, Li LX, Doering TL. 2018. Peeling the onion: the outer layers of *Cryptococcus neoformans*. Mem Inst Oswaldo Cruz 113: e180040. https://doi.org/10.1590/0074-02760180040.

30. Bulmer GS, Sans MD. 1967. *Cryptococcus neoformans*. II. Phagocytosis by human leukocytes. J Bacteriol 94:1480–1483. https://doi.org/10.1128/JB.94.5.1480-1483.1967.

31. Bulmer GS, Sans MD. 1968. *Cryptococcus neoformans*. J Bacteriol 95:5–8. https://doi.org/10.1128/JB.95.1.5-8.1968.

32. Tacker JR, Farhi F, Bulmer GS. 1972. Intracellular fate of *Cryptococcus neoformans*. Infect Immun 6:162–167. https://doi.org/10.1128/IAI.6.2.162-167.1972.

33. Monari C, Bistoni F, Vecchiarelli A. 2006. Glucuronoxylomannan exhibits potent immunosuppressive properties. FEMS Yeast Res 6:537–542. https://doi.org/10.1111/j.1567-1364.2006.00072.x.

34. Hayes JB, Sircy LM, Heusinkveld LE, Ding W, Leander RN, McClelland EE, Nelson DE. 2016. Modulation of macrophage inflammatory nuclear factor κB (NF-κB) signaling by intracellular Cryptococcus neoformans. J Biol Chem 291:15614–15627. https://doi.org/10.1074/jbc.M116.738187.

35. Fonseca FL, Nohara LL, Cordero RJB, Frases S, Casadevall A, Almeida IC, Nimrichter L, Rodrigues ML. 2010. Immunomodulatory effects of serotype B glucuronoxylomannan from Cryptococcus gattii correlate with polysaccharide diameter. Infect Immun 78:3861–3870. https://doi.org/10.1128/IAI.00111-10.

36. Garcia-Hermoso D, Dromer F, Janbon G. 2004. Cryptococcus neoformans capsule structure evolution in vitro and during murine infection. Infect Immun 72:3359–3365. https://doi.org/10.1128/IAI.72.6.3359-3365.2004.

37. Guimarães AJ, Frases S, Cordero RJB, Nimrichter L, Casadevall A, Nosanchuk JD. 2010. Cryptococcus neoformans responds to mannitol by increasing capsule size in vitro and in vivo. Cell Microbiol 12:740–753. https://doi.org/10.1111/j.1462-5822.2010.01430.x.

38. Cordero RJB, Pontes B, Guimarães AJ, Martinez LR, Rivera J, Fries BC, Nimrichter L, Rodrigues ML, Viana NB, Casadevall A. 2011. Chronological aging is associated with biophysical and chemical changes in the capsule of Cryptococcus neoformans. Infect Immun 79:4990–5000. https://doi.org/10.1128/IAI.05789-11.

39. Maier EJ, Haynes BC, Gish SR, Wang ZA, Skowyra ML, Marulli AL, Doering TL, Brent MR. 2015. Model-driven mapping of transcriptional networks reveals the circuitry and dynamics of virulence regulation. Genome Res 25:690–700. https://doi.org/10.1101/gr.184101.114.

40. Santos JRA, Holanda RA, Frases S, Bravim M, Araujo GDS, Santos PC, Costa MC, Ribeiro MJA, Ferreira GF, Baltazar LM, Miranda AS, Oliveira DB, Santos CMA, Fontes ACL, Gouveia LF, Resende-Stoianoff MA, Abrahão JS, Teixeira AL, Paixão TA, Souza DG, Santos DA. 2014. Fluconazole alters the polysaccharide capsule of Cryptococcus gattii and leads to distinct behaviors in murine cryptococcosis. PLoS One 9:e112669. https://doi.org/10.1371/journal.pone.0112669.

41. Silveira CP, Piffer AC, Kmetzsch L, Fonseca FL, Soares DA, Staats CC, Rodrigues ML, Schrank A, Vainstein MH. 2013. The heat shock protein (Hsp) 70 of Cryptococcus neoformans is associated with the fungal cell surface and influences the interaction between yeast and host cells. Fungal Genet Biol 60:53–63. https://doi.org/10.1016/j.fgb.2013.08.005.

42. Alspaugh JA. 2015. Virulence mechanisms and Cryptococcus neoformans pathogenesis. Fungal Genet Biol 78:55–58. https://doi.org/10.1016/j.fgb.2014.09.004.

43. García-Rodas R, de Oliveira H, Trevijano-Contador N, Zaragoza O. 2018. Cryptococcal Titan cells: when yeast cells are all grown up. Curr Top Microbiol Immunol 422:101–120. https://doi.org/10.1007/82_2018_145.

44. Zhou X, Ballou ER. 2018. The Cryptococcus neoformans Titan cell: from in vivo phenomenon to in vitro model. Curr Clin Micro Rpt 5:252–260. https://doi.org/10.1007/s40588-018-0107-9.

45. Zaragoza O, García-Rodas R, Nosanchuk JD, Cuenca-Estrella M, Rodríguez-Tudela JL, Casadevall A. 2010. Fungal cell gigantism during mammalian infection. PLoS Pathog 6:e1000945. https://doi.org/10.1371/journal.ppat.1000945.

46. Gerstein AC, Fu MS, Mukaremera L, Li Z, Ormerod KL, Fraser JA, Berman J, Nielsen K. 2015. Polyploid Titan cells produce haploid and aneuploid progeny to promote stress adaptation. mBio 6:e01340-15. https://doi.org/10.1128/mBio.01340-15.

47. Hommel B, Mukaremera L, Cordero RJB, Coelho C, Desjardins CA, Sturny-Leclère A, Janbon G, Perfect JR, Fraser JA, Casadevall A, Cuomo CA, Dromer F, Nielsen K, Alanio A. 2018. Titan cells formation in Cryptococcus neoformans is finely tuned by environmental conditions and modulated by positive and negative genetic regulators. PLoS Pathog 14:e1006982. https://doi.org/10.1371/journal.ppat.1006982.

48. Trevijano-Contador N, de Oliveira HC, García-Rodas R, Rossi SA, Llorente I, Zaballos Á, Janbon G, Ariño J, Zaragoza Ó. 2018. Cryptococcus neoformans can form titan-like cells in vitro in response to multiple signals. PLoS Pathog 14:e1007007. https://doi.org/10.1371/journal.ppat.1007007.

49. Dambuza IM, Drake T, Chapuis A, Zhou X, Correia J, Taylor-Smith L, LeGrave N, Rasmussen T, Fisher MC, Bicanic T, Harrison TS, Jaspars M, May RC, Brown GD, Yuecel R, MacCallum DM, Ballou ER. 2018. The Cryptococcus neoformans Titan cell is an inducible and regulated morphotype underlying pathogenesis. PLoS Pathog 14:e1006978. https://doi.org/10.1371/journal.ppat.1006978.

50. García-Barbazán I, Trevijano-Contador N, Rueda C, de Andrés B, Pérez-Tavárez R, Herrero-Fernández I, Gaspar ML, Zaragoza O. 2016. The formation of titan cells in Cryptococcus neoformans depends on the mouse strain and correlates with induction of Th2-type responses. Cell Microbiol 18:111–124. https://doi.org/10.1111/cmi.12488.

51. Mukaremera L, Lee KK, Wagener J, Wiesner DL, Gow NAR, Nielsen K. 2018. Titan cell production in Cryptococcus neoformans reshapes the cell wall and capsule composition during infection. Cell Surf 1:15–24. https://doi.org/10.1016/j.tcsw.2017.12.001.

52. Jung K-W, Yang D-H, Maeng S, Lee K-T, So Y-S, Hong J, Choi J, Byun H-J, Kim H, Bang S, Song M-H, Lee J-W, Kim MS, Kim S-Y, Ji J-H, Park G, Kwon H, Cha S, Meyers GL, Wang LL, Jang J, Janbon G, Adedoyin G, Kim T, Averette AK, Heitman J, Cheong E, Lee Y-H, Lee Y-W, Bahn Y-S. 2015. Systematic functional profiling of transcription factor networks in Cryptococcus neoformans. Nat Commun 6:6757. https://doi.org/10.1038/ncomms7757.

53. Schneider R, de O, Fogaça N, de SS, Kmetzsch L, Schrank A, Vainstein MH, Staats CC. 2012. Zap1 regulates zinc homeostasis and modulates virulence in Cryptococcus gattii. PLoS One 7:e43773. https://doi.org/10.1371/journal.pone.0043773.

54. Garcia-Santamarina S, Festa RA, Smith AD, Yu C-H, Probst C, Ding C, Homer CM, Yin J, Noonan JP, Madhani H, Perfect JR, Thiele DJ. 2018. Genome-wide analysis of the regulation of Cu metabolism in Cryptococcus neoformans. Mol Microbiol 108:473–494. https://doi.org/10.1111/mmi.13960.

55. Lev S, Kaufman-Francis K, Desmarini D, Juillard PG, Li C, Stifter SA, Feng CG, Sorrell TC, Grau GER, Bahn Y-S, Djordjevic JT. 2017. Pho4 is essential for dissemination of Cryptococcus neoformans to the host brain by promoting phosphate uptake and growth at alkaline pH. mSphere 2:e00381-16. https://doi.org/10.1128/mSphere.00381-16.

56. Jung WH, Sham A, White R, Kronstad JW. 2006. Iron regulation of the major virulence factors in the AIDS-associated pathogen Cryptococcus neoformans. PLoS Biol 4:e410. https://doi.org/10.1371/journal.pbio.0040410.

57. Chow EWL, Clancey SA, Billmyre RB, Averette AF, Granek JA, Mieczkowski P, Cardenas ME, Heitman J. 2017. Elucidation of the calcineurin-Crz1 stress response transcriptional network in the human fungal pathogen Cryptococcus neoformans. PLoS Genet 13:e1006667. https://doi.org/10.1371/journal.pgen.1006667.

58. O'Meara TR, Norton D, Price MS, Hay C, Clements MF, Nichols CB, Alspaugh JA. 2010. Interaction of Cryptococcus neoformans Rim101 and protein kinase A regulates capsule. PLoS Pathog 6:e1000776. https://doi.org/10.1371/journal.ppat.1000776.

59. Gish SR, Maier EJ, Haynes BC, Santiago-Tirado FH, Srikanta DL, Ma CZ, Li LX, Williams M, Crouch EC, Khader SA, Brent MR, Doering TL. 2016. Computational analysis reveals a key regulator of cryptococcal virulence and determinant of host response. mBio 7:e00313-16. https://doi.org/10.1128/mBio.00313-16.

60. Chun CD, Brown JCS, Madhani HD. 2011. A major role for capsule-independent phagocytosis-inhibitory mechanisms in mammalian infection by Cryptococcus neoformans. Cell Host Microbe 9:243–251. https://doi.org/10.1016/j.chom.2011.02.003.

61. Moranova Z, Virtudazo E, Hricova K, Ohkusu M, Kawamoto S, Husickova V, Raclavsky V. 2014. The CRZ1/SP1-like gene links survival under limited aeration, cell integrity and biofilm formation in the pathogenic yeast Cryptococcus neoformans. Biomed Pap Med Fac Univ Palacky Olomouc Czech Repub 158:212–220. https://doi.org/10.5507/bp.2013.024.

62. Lev S, Desmarini D, Chayakulkeeree M, Sorrell TC, Djordjevic JT. 2012. The Crz1/Sp1 transcription factor of Cryptococcus neoformans is activated by calcineurin and regulates cell wall integrity. PLoS One 7:e51403. https://doi.org/10.1371/journal.pone.0051403.

63. Park HS, Chow EWL, Fu C, Soderblom EJ, Moseley MA, Heitman J, Cardenas ME. 2016. Calcineurin targets involved in stress survival and fungal virulence. PLoS Pathog 12:e1005873. https://doi.org/10.1371/journal.ppat.1005873.

64. Lee D, Jang E-H, Lee M, Kim S-W, Lee Y, Lee K-T, Bahn Y-S. 2019. Unraveling melanin biosynthesis and signaling networks in Cryptococcus neoformans. mBio 10:e02267-19. https://doi.org/10.1128/mBio.02267-19.

65. Rhodes J, Desjardins CA, Sykes SM, Beale MA, Vanhove M, Sakthikumar S, Chen Y, Gujja S, Saif S, Chowdhary A, Lawson DJ, Ponzio V, Colombo AL, Meyer W, Engelthaler DM, Hagen F, Illnait-Zaragozi MT, Alanio A, Vreulink J-M, Heitman J, Perfect JR, Litvintseva AP, Bicanic T, Harrison TS, Fisher MC, Cuomo CA. 2017. Tracing genetic exchange and biogeography of Cryptococcus neoformans var. grubii at the global population level. Genetics 207:327–346. https://doi.org/10.1534/genetics.117.203836.

66. Liu OW, Chun CD, Chow ED, Chen C, Madhani HD, Noble SM. 2008. Systematic genetic analysis of virulence in the human fungal pathogen Cryptococcus neoformans. Cell 135:174–188. https://doi.org/10.1016/j.cell.2008.07.046.

67. Lee K-T, Hong J, Lee D-G, Lee M, Cha S, Lim Y-G, Jung K-W, Hwangbo A, Lee Y, Yu S-J, Chen Y-L, Lee J-S, Cheong E, Bahn Y-S. 2020. Fungal kinases and

transcription factors regulating brain infection in *Cryptococcus neoformans*. Nat Commun 11:1521. https://doi.org/10.1038/s41467-020-15329-2.

68. Krysan DJ, Zhai B, Beattie SR, Misel KM, Wellington M, Lin X. 2019. Host carbon dioxide concentration is an independent stress for *Cryptococcus neoformans* that affects virulence and antifungal Susceptibility. mBio 10: e01410-19. https://doi.org/10.1128/mBio.01410-19.

69. D'Souza CA, Alspaugh JA, Yue C, Harashima T, Cox GM, Perfect JR, Heitman J. 2001. Cyclic AMP-dependent protein kinase controls virulence of the fungal pathogen *Cryptococcus neoformans*. Mol Cell Biol 21:3179–3191. https://doi.org/10.1128/MCB.21.9.3179-3191.2001.

70. Hu G, Steen BR, Lian T, Sham AP, Tam N, Tangen KL, Kronstad JW. 2007. Transcriptional regulation by protein kinase A in *Cryptococcus neoformans*. PLoS Pathog 3:e42. https://doi.org/10.1371/journal.ppat.0030042.

71. Yoneda A, Doering TL. 2008. Regulation of *Cryptococcus neoformans* capsule size is mediated at the polymer level. Eukaryot Cell 7:546–549. https://doi.org/10.1128/EC.00437-07.

72. Frases S, Pontes B, Nimrichter L, Viana NB, Rodrigues ML, Casadevall A. 2009. Capsule of *Cryptococcus neoformans* grows by enlargement of polysaccharide molecules. Proc Natl Acad Sci U S A 106:1228–1233. https://doi.org/10.1073/pnas.0808995106.

73. Gaylord EA, Choy HL, Doering TL. 2020. Dangerous liaisons: interactions of *Cryptococcus neoformans* with host phagocytes. Pathogens 9:891. https://doi.org/10.3390/pathogens9110891.

74. Summers DK, Perry DS, Rao B, Madhani HD. 2020. Coordinate genomic association of transcription factors controlled by an imported quorum sensing peptide in *Cryptococcus neoformans*. PLoS Genet 16:e1008744. https://doi.org/10.1371/journal.pgen.1008744.

75. Homer CM, Summers DK, Goranov AI, Clarke SC, Wiesner DL, Diedrich JK, Moresco JJ, Toffaletti D, Upadhya R, Caradonna I, Petnic S, Pessino V, Cuomo CA, Lodge JK, Perfect J, Yates JR, III, Nielsen K, Craik CS, Madhani HD. 2016. Intracellular action of a secreted peptide required for fungal virulence. Cell Host Microbe 19:849–864. https://doi.org/10.1016/j.chom.2016.05.001.

76. Bailey TL. 2011. DREME: motif discovery in transcription factor ChIP-seq data. Bioinformatics 27:1653–1659. https://doi.org/10.1093/bioinformatics/btr261.

77. Kang Y, Patel NR, Shively C, Recio PS, Chen X, Wranik BJ, Kim G, Scott McIsaac R, Mitra R, Brent MR. 2020. Dual threshold optimization and network inference reveal convergent evidence from TF binding locations and TF perturbation responses. Genome Res 30:459–471. https://doi.org/10.1101/gr.259655.119.

78. Giles SS, Stajich JE, Nichols C, Gerrald QD, Alspaugh JA, Dietrich F, Perfect JR. 2006. The *Cryptococcus neoformans* catalase gene family and its role in antioxidant defense. Eukaryot Cell 5:1447–1459. https://doi.org/10.1128/EC.00098-06.

79. Cox GM, Harrison TS, McDade HC, Taborda CP, Heinrich G, Casadevall A, Perfect JR. 2003. Superoxide dismutase influences the virulence of *Cryptococcus neoformans* by affecting growth within macrophages. Infect Immun 71:173–180. https://doi.org/10.1128/iai.71.1.173-180.2003.

80. Lee K-T, So Y-S, Yang D-H, Jung K-W, Choi J, Lee D-G, Kwon H, Jang J, Wang LL, Cha S, Meyers GL, Jeong E, Jin J-H, Lee Y, Hong J, Bang S, Ji J-H, Park G, Byun H-J, Park SW, Park Y-M, Adedoyin G, Kim T, Averette AF, Choi J-S, Heitman J, Cheong E, Lee Y-H, Bahn Y-S. 2016. Systematic functional analysis of kinases in the fungal pathogen *Cryptococcus neoformans*. Nat Commun 7:12766. https://doi.org/10.1038/ncomms12766.

81. Caza M, Hu G, Price M, Perfect JR, Kronstad JW. 2016. The zinc finger protein Mig1 regulates mitochondrial function and azole drug susceptibility in the pathogenic fungus *Cryptococcus neoformans*. mSphere 1:e00080-15. https://doi.org/10.1128/mSphere.00080-15.

82. Chen Y, Toffaletti DL, Tenor JL, Litvintseva AP, Fang C, Mitchell TG, McDonald TR, Nielsen K, Boulware DR, Bicanic T, Perfect JR. 2014. The *Cryptococcus neoformans* transcriptome at the site of human meningitis. mBio 5:e01087-13. https://doi.org/10.1128/mBio.01087-13.

83. Alspaugh JA, Pukkila-Worley R, Harashima T, Cavallo LM, Funnell D, Cox GM, Perfect JR, Kronstad JW, Heitman J. 2002. Adenylyl cyclase functions downstream of the Gα protein Gpa1 and controls mating and pathogenicity of *Cryptococcus neoformans*. Eukaryot Cell 1:75–84. https://doi.org/10.1128/ec.1.1.75-84.2002.

84. Heung LJ, Kaiser AE, Luberto C, Del Poeta M. 2005. The role and mechanism of diacylglycerol-protein kinase C1 signaling in melanogenesis by *Cryptococcus neoformans*. J Biol Chem 280:28547–28555. https://doi.org/10.1074/jbc.M503404200.

85. Gerik KJ, Bhimireddy SR, Ryerse JS, Specht CA, Lodge JK. 2008. PKC1 is essential for protection against both oxidative and nitrosative stresses, cell integrity, and normal manifestation of virulence factors in the pathogenic fungus

Cryptococcus neoformans. Eukaryot Cell 7:1685–1698. https://doi.org/10.1128/EC.00146-08.

86. Waterman SR, Hacham M, Hu G, Zhu X, Park Y-D, Shin S, Panepinto J, Valyi-Nagy T, Beam C, Husain S, Singh N, Williamson PR. 2007. Role of a CUF1/CTR4 copper regulatory axis in the virulence of *Cryptococcus neoformans*. J Clin Invest 117:794–802. https://doi.org/10.1172/JCI30006.

87. Jiang N, Sun N, Xiao D, Pan J, Wang Y, Zhu X. 2009. A copper-responsive factor gene *CUF1* required for copper induction of laccase in *Cryptococcus neoformans*. FEMS Microbiol Lett 296:84–90. https://doi.org/10.1111/j.1574-6968.2009.01619.x.

88. Walton FJ, Idnurm A, Heitman J. 2005. Novel gene functions required for melanization of the human pathogen *Cryptococcus neoformans*. Mol Microbiol 57:1381–1396. https://doi.org/10.1111/j.1365-2958.2005.04779.x.

89. Cheon SA, Jung K-W, Chen Y-L, Heitman J, Bahn Y-S, Kang HA. 2011. Unique evolution of the UPR pathway with a novel bZIP transcription factor, Hxl1, for controlling pathogenicity of *Cryptococcus neoformans*. PLoS Pathog 7:e1002177. https://doi.org/10.1371/journal.ppat.1002177.

90. Hicks JK, Bahn YS, Heitman J. 2005. Pde1 phosphodiesterase modulates cyclic AMP levels through a protein kinase A-mediated negative feedback loop in *Cryptococcus neoformans*. Eukaryot Cell 4:1971–1981. https://doi.org/10.1128/EC.4.12.1971-1981.2005.

91. Kozubowski L, Lee SC, Heitman J. 2009. Signalling pathways in the pathogenesis of *Cryptococcus*. Cell Microbiol 11:370–380. https://doi.org/10.1111/j.1462-5822.2008.01273.x.

92. Fox DS, Cruz MC, Sia RAL, Ke H, Cox GM, Cardenas ME, Heitman J. 2001. Calcineurin regulatory subunit is essential for virulence and mediates interactions with FKBP12-FK506 in *Cryptococcus neoformans*. Mol Microbiol 39:835–849. https://doi.org/10.1046/j.1365-2958.2001.02295.x.

93. Odom A, Muir S, Lim E, Toffaletti DL, Perfect J, Heitman J. 1997. Calcineurin is required for virulence of *Cryptococcus neoformans*. EMBO J 16:2576–2589. https://doi.org/10.1093/emboj/16.10.2576.

94. Jung W-H, Son Y-E, Oh S-H, Fu C, Kim HS, Kwak J-H, Cardenas ME, Heitman J, Park HS. 2018. Had1 is required for cell wall integrity and fungal virulence in *Cryptococcus neoformans*. G3 (Bethesda) 8:643–652. https://doi.org/10.1534/g3.117.300444.

95. Kmetzsch L, Staats CC, Cupertino JB, Fonseca FL, Rodrigues ML, Schrank A, Vainstein MH. 2013. The calcium transporter Pmc1 provides Ca2+ tolerance and influences the progression of murine cryptococcal infection. FEBS J 280:4853–4864. https://doi.org/10.1111/febs.12458.

96. Kmetzsch L, Staats CC, Simon E, Fonseca FL, de Oliveira DL, Sobrino L, Rodrigues J, Leal AL, Nimrichter L, Rodrigues ML, Schrank A, Vainstein MH. 2010. The vacuolar Ca2+ exchanger Vcx1 is involved in calcineurin-dependent Ca2+ tolerance and virulence in *Cryptococcus neoformans*. Eukaryot Cell 9:1798–1805. https://doi.org/10.1128/EC.00114-10.

97. Denham S, Brown J. 2018. Mechanisms of pulmonary escape and dissemination by *Cryptococcus neoformans*. J Fungi (Basel) 4:25. https://doi.org/10.3390/jof4010025.

98. Sun D, Sun P, Li H, Zhang M, Liu G, Strickland AB, Chen Y, Fu Y, Xu J, Yosri M, Nan Y, Zhou H, Zhang X, Shi M. 2019. Fungal dissemination is limited by liver macrophage filtration of the blood. Nat Commun 10:4566. https://doi.org/10.1038/s41467-019-12381-5.

99. Santiago-Tirado FH, Doering TL. 2017. False friends: phagocytes as Trojan horses in microbial brain infections. PLoS Pathog 13:e1006680. https://doi.org/10.1371/journal.ppat.1006680.

100. Squizani ED, Oliveira NK, Reuwsaat JCV, Marques BM, Lopes W, Gerber AL, de Vasconcelos ATR, Lev S, Djordjevic JT, Schrank A, Vainstein MH, Staats CC, Kmetzsch L. 2018. Cryptococcal dissemination to the central nervous system requires the vacuolar calcium transporter Pmc1. Cell Microbiol 20:e12803. https://doi.org/10.1111/cmi.12803.

101. Okagaki LH, Nielsen K. 2012. Titan cells confer protection from phagocytosis in *Cryptococcus neoformans* infections. Eukaryot Cell 11:820–826. https://doi.org/10.1128/EC.00121-12.

102. Srikanta D, Santiago-Tirado FH, Doering TL. 2014. *Cryptococcus neoformans*: historical curiosity to modern pathogen. Yeast 31:47–60. https://doi.org/10.1002/yea.2997.

103. Nielsen K, Cox GM, Wang P, Toffaletti DL, Perfect JR, Heitman J. 2003. Sexual cycle of *Cryptococcus neoformans* var. *grubii* and virulence of congenic a and α isolates. Infect Immun 71:4831–4841. https://doi.org/10.1128/iai.71.9.4831-4841.2003.

104. Reuwsaat JCV, Motta H, Garcia AWA, Vasconcelos CB, Marques BM, Oliveira NK, Rodrigues J, Ferrareze PAG, Frases S, Lopes W, Barcellos VA, Squizani ED, Horta JA, Schrank A, Rodrigues ML, Staats CC, Vainstein MH, Kmetzsch L. 2018. A predicted mannoprotein participates in *Cryptococcus*

gattii capsular structure. mSphere 3:e00023-18. https://doi.org/10.1128/mSphere.00023-18.

105. Haynes BC, Skowyra ML, Spencer SJ, Gish SR, Williams M, Held EP, Brent MR, Doering TL. 2011. Toward an integrated model of capsule regulation in *Cryptococcus neoformans*. PLoS Pathog 7:e1002411. https://doi.org/10.1371/journal.ppat.1002411.

106. Denham ST, Brammer B, Chung KY, Wambaugh MA, Bednarek J, Guo L, Brown JCS. 2020. Phosphate induces a morphological shift that enhances vascular dissemination of *Cryptococcus neoformans*. bioRxiv 2020.08.27.270843.

107. Babraham Bioinformatics. FastQC: a quality control tool for high throughput sequence data. https://www.bioinformatics.babraham.ac.uk/projects/fastqc/. Accessed 24 June 2019.

108. Friedman RZ, Gish SR, Brown H, Brier L, Howard N, Doering TL, Brent MR. 2018. Unintended side effects of transformation are very rare in *Cryptococcus neoformans*. G3 (Bethesda) 8:815–822. https://doi.org/10.1534/g3.117.300357.

109. Sedlazeck FJ, Rescheneder P, von Haeseler A. 2013. NextGenMap: fast and accurate read mapping in highly polymorphic genomes. Bioinformatics 29:2790–2791. https://doi.org/10.1093/bioinformatics/btt468.

110. Li H, Handsaker B, Wysoker A, Fennell T, Ruan J, Homer N, Marth G, Abecasis G, Durbin R, 1000 Genome Project Data Processing Subgroup. 2009. The Sequence Alignment/Map format and SAMtools. Bioinformatics 25:2078–2079. https://doi.org/10.1093/bioinformatics/btp352.

111. Zhang Y, Liu T, Meyer CA, Eeckhoute J, Johnson DS, Bernstein BE, Nusbaum C, Myers RM, Brown M, Li W, Liu XS. 2008. Model-based analysis of ChIP-Seq (MACS). Genome Biol 9:R137. https://doi.org/10.1186/gb-2008-9-9-r137.

112. Heinz S, Benner C, Spann N, Bertolino E, Lin YC, Laslo P, Cheng JX, Murre C, Singh H, Glass CK. 2010. Simple combinations of lineage-determining transcription factors prime cis-regulatory elements required for macrophage and B cell identities. Mol Cell 38:576–589. https://doi.org/10.1016/j.molcel.2010.05.004.

113. Novocraft Technologies. 2014. NovoAlign. http://www.novocraft.com/. Accessed 25 November 2020.

114. Anders S, Pyl PT, Huber W. 2015. HTSeq–a Python framework to work with high-throughput sequencing data. Bioinformatics 31:166–169. https://doi.org/10.1093/bioinformatics/btu638.

115. Love MI, Huber W, Anders S. 2014. Moderated estimation of fold change and dispersion for RNA-seq data with DESeq2. Genome Biol 15:550. https://doi.org/10.1186/s13059-014-0550-8.

116. Ignatiadis N, Klaus B, Zaugg JB, Huber W. 2016. Data-driven hypothesis weighting increases detection power in genome-scale multiple testing. Nat Methods 13:577–580. https://doi.org/10.1038/nmeth.3885.

117. Li LX, Rautengarten C, Heazlewood JL, Doering TL. 2018. Xylose donor transport is critical for fungal virulence. PLoS Pathog 14:e1006765. https://doi.org/10.1371/journal.ppat.1006765.

118. Janbon G, Ormerod KL, Paulet D, Byrnes EJ, Yadav V, Chatterjee G, Mullapudi N, Hon C-C, Billmyre RB, Brunel F, Bahn Y-S, Chen W, Chen Y, Chow EWL, Coppée J-Y, Floyd-Averette A, Gaillardin C, Gerik KJ, Goldberg J, Gonzalez-Hilarion S, Gujja S, Hamlin JL, Hsueh Y-P, Ianiri G, Jones S, Kodira CD, Kozubowski L, Lam W, Marra M, Mesner LD, Mieczkowski PA, Moyrand F, Nielsen K, Proux C, Rossignol T, Schein JE, Sun S, Wollschlaeger C, Wood IA, Zeng Q, Neuvéglise C, Newlon CS, Perfect JR, Lodge JK, Idnurm A, Stajich JE, Kronstad JW, Sanyal K, Heitman J, Fraser JA, Cuomo CA, Dietrich FS. 2014. Analysis of the genome and transcriptome of *Cryptococcus neoformans* var. *grubii* reveals complex RNA expression and microevolution leading to virulence attenuation. PLoS Genet 10:e1004261. https://doi.org/10.1371/journal.pgen.1004261.